Materials for the Green Energy Economy

By Prof. Dr. Rolando M.A. Roque-Malherbe

Institute of Physical-Chemical Applied Research,
School of Science,
University of Turabo,
Ana G. Méndez University System,
Puerto Rico,
USA.

Universidad del Turabo

June 1, 2007

The Institute of Physical-Chemical Applied Research

The Institute of Physical-Chemical Applied Research (IPCAR) supports the USA's commitment to achieve a broad-based research capability in the development of new materials for Energy Applications, Pollution Abatement, and the Development of Sensors for Nuclear Safety

IPCAR Research Staff

The IPCAR staff is composed of three full time senior researchers: Rolando Roque-Malherbe, PhD and Santander Nieto, PhD, the third position is under the hiring process. Two half time Research Assistants (RA), Maria Cotto, MSc, and the other RA position to be filled. Three part time senior researchers: Jose Duconge, PhD; Rodulio Caudales, PhD and Marlio Paredes, PhD, and two part time Research Associates: Carlos Neira, BSc and Francisco Diaz, MSc Besides, in the group are currently working two undergraduate students and two graduate students.

IPCAR Concrete Objectives

Conduct innovative R&D projects in the synthesis, modification and characterization of zeolites, silicas, and perovskites for the hydrogen and ethanol economies, pollution abatement, development of sensors for nuclear safety. This endeavor is carried out in order to participate in the USA's Hydrogen and Ethanol-related science programs. The efforts in Pollution Abatement and the USA's commitment in the development of safe Nuclear Applications.

Current Research Projects

- Hydrogen production by water splitting.
- Synthesis and characterization of proton conducting perovskites for hydrogen and oxygen cleaning.
- Dense and Porous Membrane Synthesis.
- Hydrogen production with a plasma torch.
- Development of silica xerogels with extremely high surface area to be used as storage systems for hydrogen using ammonia as the molecular support.
- Production of synthetic and natural zeolites for heavy metal removal from waste waters.
- Development of a silica aerogel for the creation of a Cherenkov Counter, and as well other sensors.

Hydrogen Production by Water Splitting

Hydrogen production by water splitting is developed around the project entitled “Solar Water Splitting with Quantum Boost”. In order to develop this project was assembled an excellent team composed of researchers from: Science Applications International Corporation (SAIC), San Diego, CA, the Florida Solar Energy Center at University of Central Florida (FSEC-UCF), Cocoa Beach, FL and the IPCAR at UT. This project was awarded by the Department of Energy.

Water Splitting Process with Quantum Boost

The approach that will be used is based on splitting water using a two-step high-temperature cycle that include one step utilizing solar (visible and/or near-UV) photons according to the following scheme [1]:

$CO_2 + \text{heat}/h\nu \rightarrow CO + \frac{1}{2} O_2 \quad \Delta H^o = 283 \text{ kJ/mol} \quad (1)$

$CO + H_2O \rightarrow CO_2 + H_2 \quad \Delta H^o = -41 \text{ kJ/mol} \quad (2)$

A quantum boost exercised by the solar near-UV and visible photons conducts to CO_2 thermal dissociation at the temperature range of 1500-2500 K easily attainable by solar concentrators. In addition reaction "2" is the very well-known water gas shift reaction

1. R. Taylor, C. Mullich, A. Raissi and R. Roque-Malherbe, Solar High-Temperature Water-Splitting Cycle With Quantum Boost, Solicitation Number DE-PS36-03GO093007, to the Department of Energy Program: Hydrogen Production Using High Temperature Thermochemical Water Splitting Cycles, SAIC-FSEC-UT, 2004.

CO_2 Absorption Spectra at 298 and 2273 K

$CO_2 + h\nu \rightarrow CO + \frac{1}{2} O_2$ $\quad \Delta H^\circ = 283$ kJ/mol

$CO + H_2O \rightarrow CO_2 + H_2$ $\quad \Delta H^\circ = -41$ kJ/mol

Despite the fact that the enthalpy of CO_2 dissociation reaction is higher than that of water ($2\ H_2O \leftrightarrow 2\ H_2 + O_2$, $\Delta H^o = 242$ kJ/mol) the CO_2 molecule exhibits two very important attributes that make this cycle particularly Attractive. The first is that the CO_2 molecules absorb photons in the UV region, present in the solar spectrum, at high temperature (see the figure) and consequently a certain amount of Gibbs free energy can be added to the system in the form of photon energy [1].

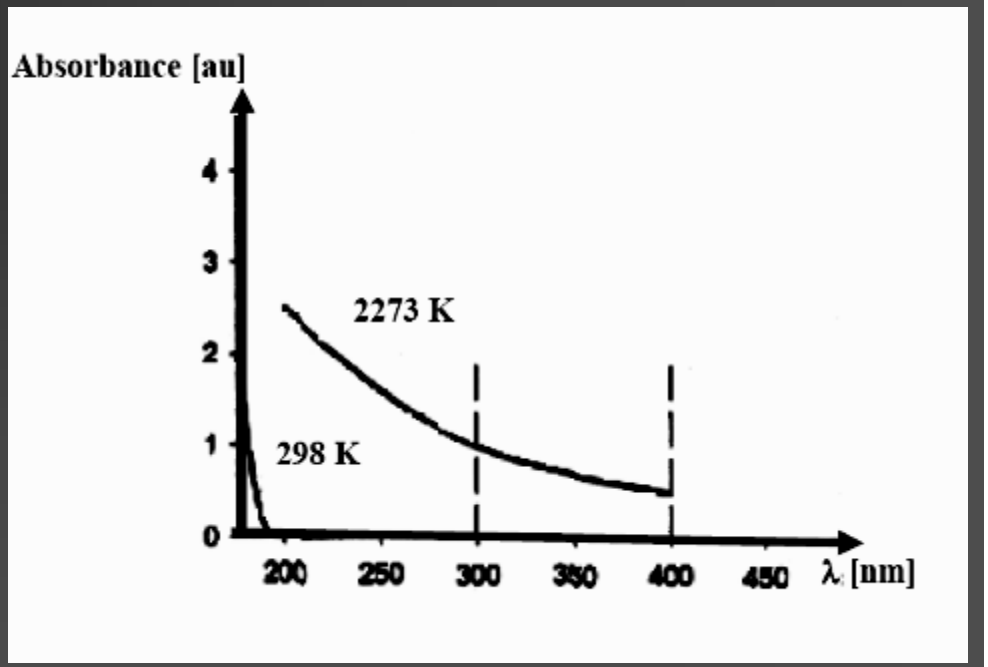

Thermodynamics of the CO_2 and H_2O Dissociation Reactions

$CO_2 + h\nu \rightarrow CO + \frac{1}{2} O_2$	$\Delta H^\circ = 283$ kJ/mol
$CO + H_2O \rightarrow CO_2 + H_2$	$\Delta H^\circ = -41$ kJ/mol

The second attribute is that the energy requirements, at high temperature, for both dissociation reactions, are more favorable in the case of CO_2 (see the figure); since the reaction "1" has a larger thermal ($T\Delta S$) component of the total enthalpy ($\Delta H = \Delta G + T\Delta S$), compared to water [1]

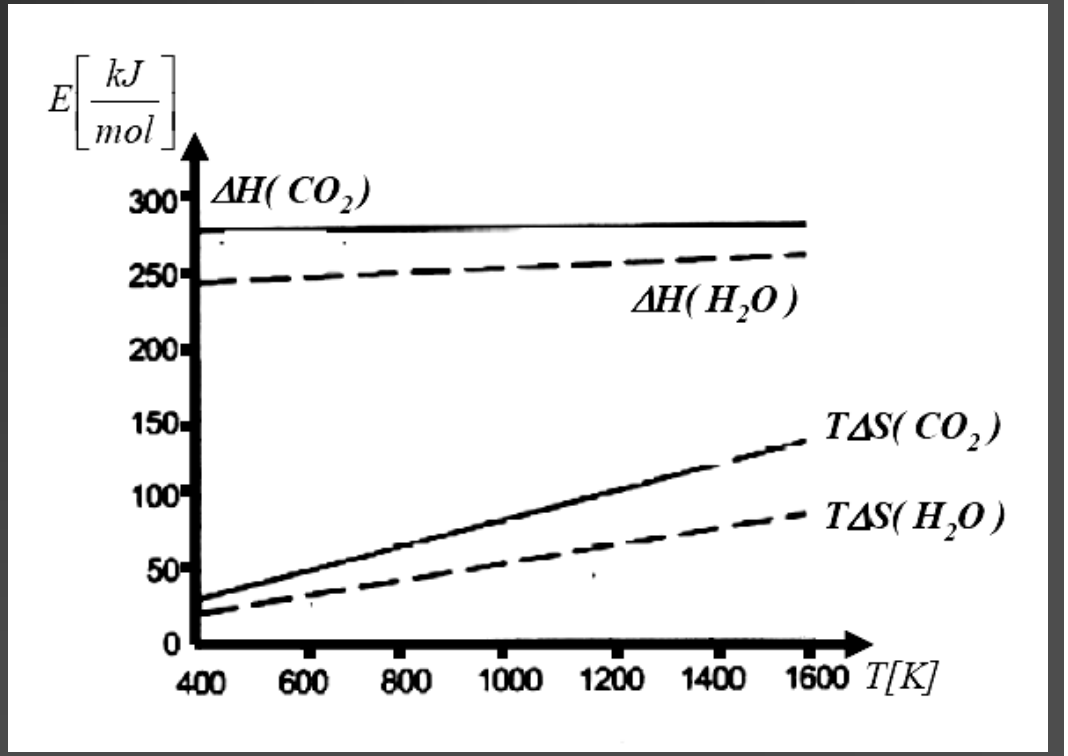

1. R. Taylor, C. Mullich, A. Raissi and R. Roque-Malherbe, Solar High-Temperature Water-Splitting Cycle With Quantum Boost, Solicitation Number DE-PS36-03GO093007, to the Department of Energy Program: Hydrogen Production Using High Temperature Thermochemical Water Splitting Cycles, SAIC-FSEC-UT, 2004.

CO_2 Cycle for Water Splitting with Quantum Boost [1]

The energy requirement for the dissociation reaction is more propitious in the case of CO_2 than for water, since reaction 1 has a larger thermal, $T\Delta S$, component of the total energy, ΔH, than the water dissociation reaction. Second, at high temperatures, that is, larger that 1500 K, CO_2 becomes susceptible to near-UV and even visible light. This results in CO_2 thermal dissociation at a temperature range between 2000-2500 K, that is a span readily achievable in state-of-the-art solar concentrators such as those developed by SAIC.

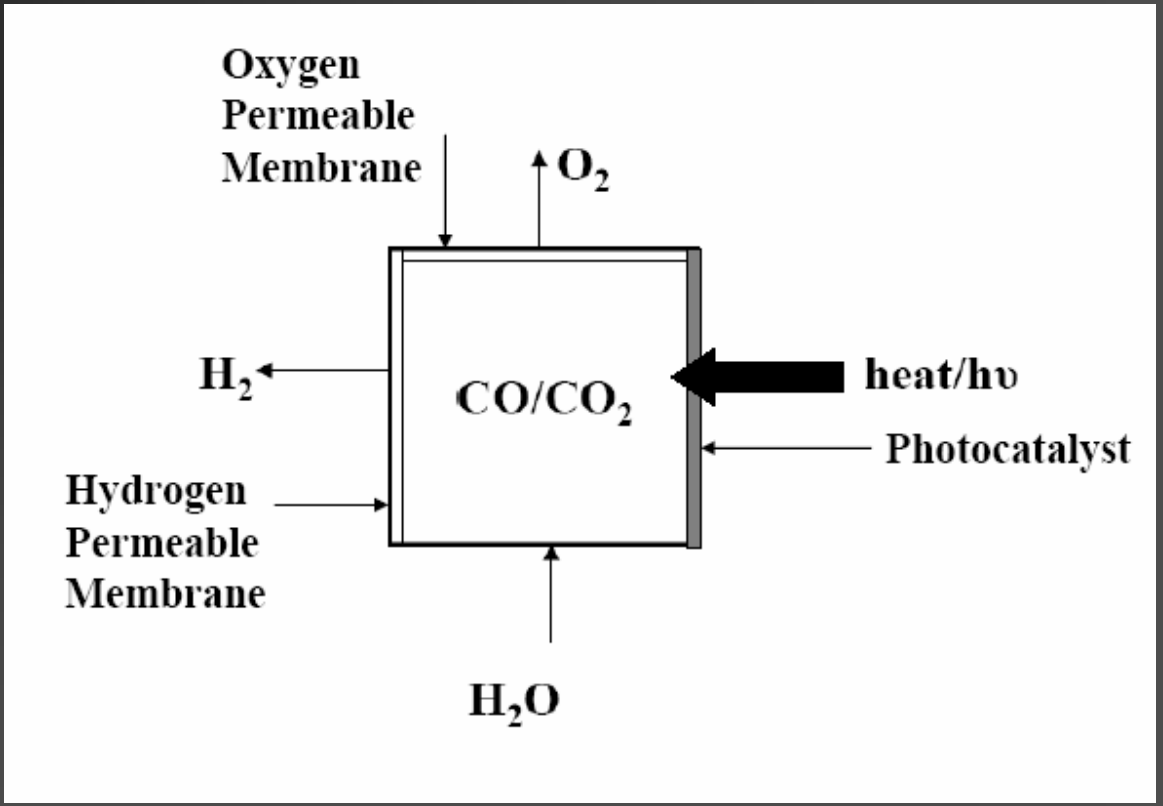

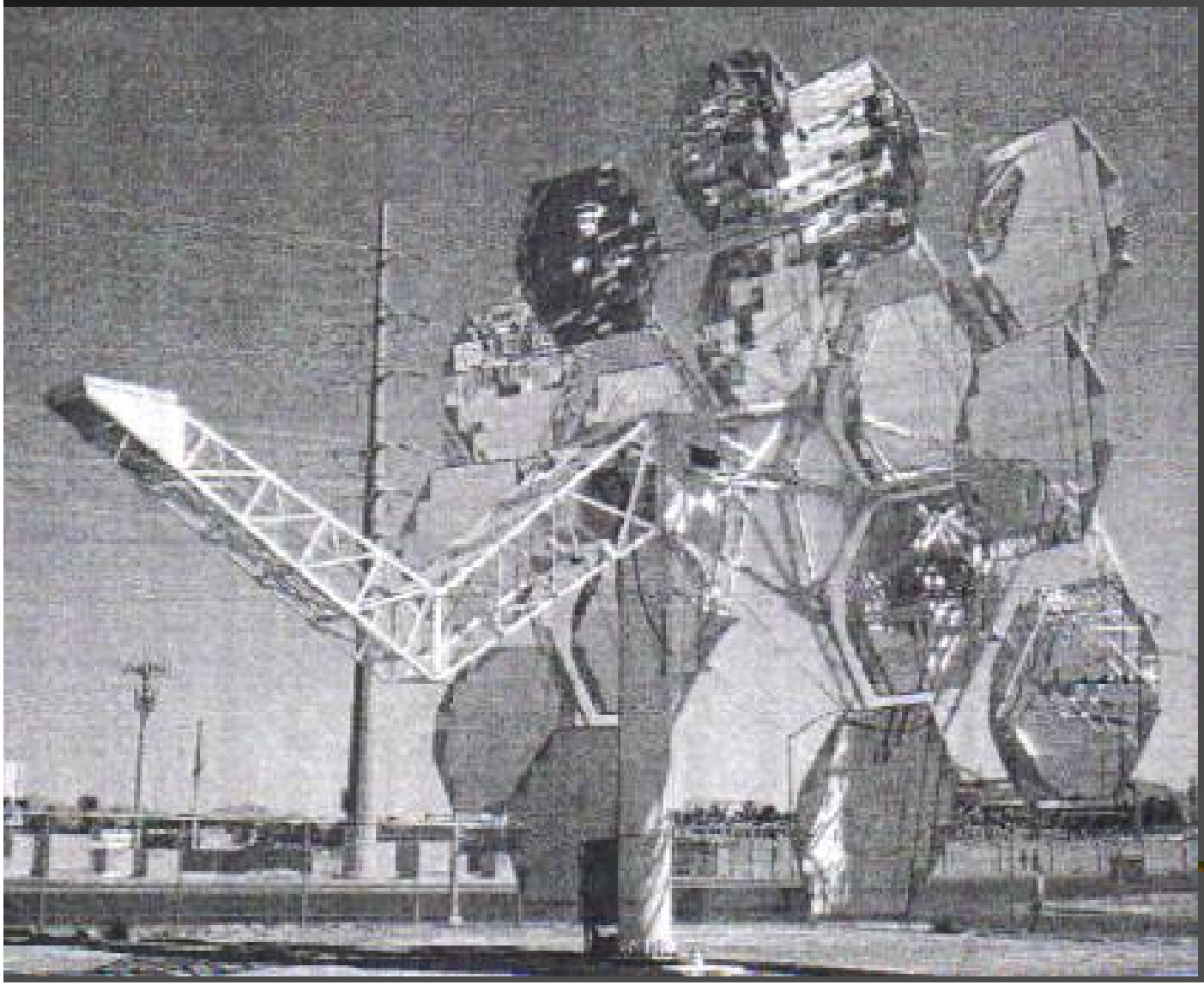

SAIC Dish Concentrator System

Schematic Diagram Describing the Solar-powered Process for High-temperature Water Splitting [1]

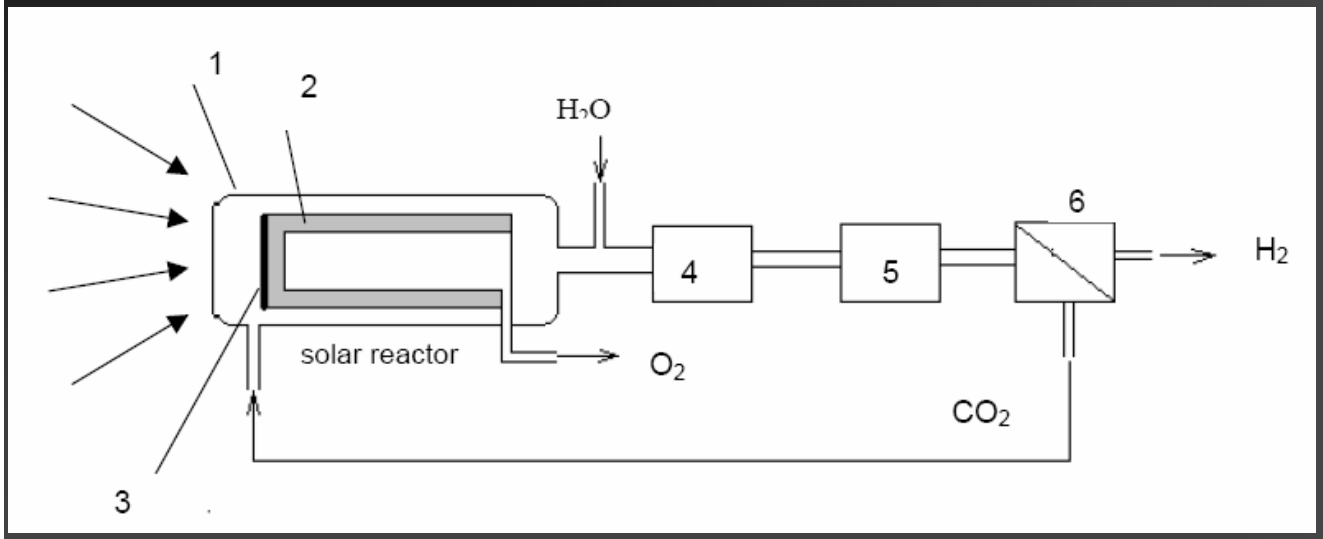

Where: 1- quartz window, 2- ceramic oxygen-permeable membrane, 3- catalyst, 4- turbine, 5- water gas shift reactor, 6-hydrogen-permeable membrane

1. R. Taylor, C. Mullich, A. Raissi and R. Roque-Malherbe, Solar High-Temperature Water-Splitting Cycle With Quantum Boost, Solicitation Number DE-PS36-03GO093007, to the Department of Energy Program: Hydrogen Production Using High Temperature Thermochemical Water Splitting Cycles, SAIC-FSEC-UT, 2004.

Phase 1:

Where:
1-quartz window,
2- ceramic oxygen-permeable membrane and
3- catalyst.

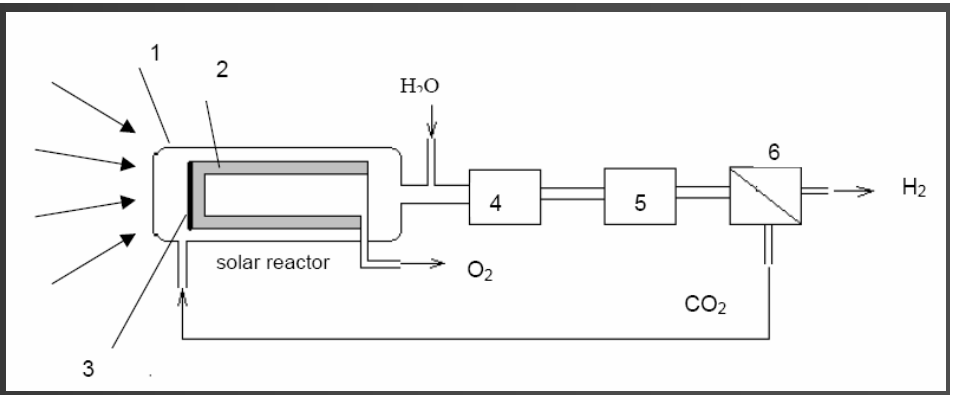

A directly irradiated solar reactor with a quartz window and an oxygen permeable ceramic membrane coated with a photocatalyst. This photocatalyst/membrane arrangement is exposed to concentrated solar radiation. The ceramic oxygen-permeable membrane further accelerates the process of CO_2 decomposition by shifting reaction equilibrium and preventing the reverse reaction. The function of the photocatalyst is to enhance the kinetics of CO_2 dissociation via an interaction with the active sites, leading to weakening of C = O bonds [1].

1. R. Taylor, C. Mullich, A. Raissi and R. Roque-Malherbe, Solar High-Temperature Water-Splitting Cycle With Quantum Boost, Solicitation Number DE-PS36-03GO093007, to the Department of Energy Program: Hydrogen Production Using High Temperature Thermochemical Water Splitting Cycles, SAIC-FSEC-UT, 2004.

Catalyst-membrane Arrangement [1]

The figure depicts the proposed catalyst-membrane arrangement for high-temperature solar-driven decomposition of CO_2. Upon exposure to light, both near UV and visible, at high temperatures, CO_2 molecules dissociate over the surface of a thin photocatalyst layer immobilized onto an O_2-permeable ceramic membrane where oxygen atoms (or molecules) generated at the surface, then permeate through the membrane in the direction of decreasing oxygen chemical potential.

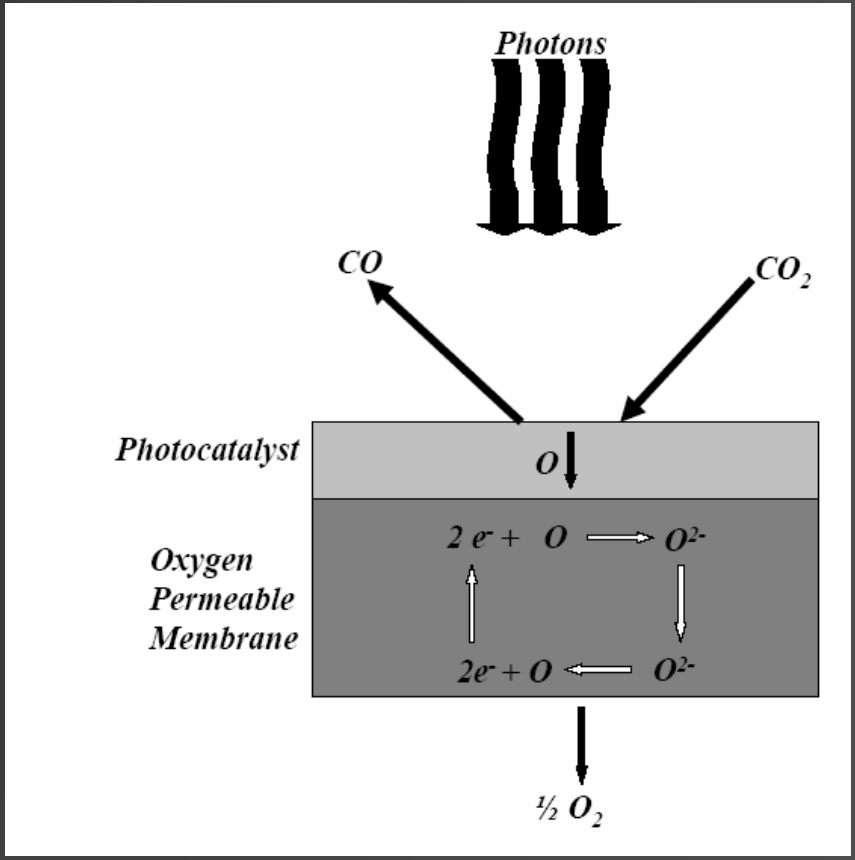

The non-permeate gases (CO and unconverted CO_2) bypass the membrane and leave the reaction zone via a valve that regulates the flow and maintains the required pressure drop for oxygen permeation.

Mechanism of the Photocatalyst Process

The effect of the photocatalyst and the photons is to generate an excited charge-transfer state that reacts with an adsorbed CO_2 molecule dissociating the molecule according to the following scheme [1] :

$$M^{n+} = O^{2-} + h\upsilon \rightarrow \left(M^{(n-1)+} - O^{-}\right)^{*} \rightarrow M^{n+} = O^{2-}$$

$$O = C = O \rightarrow O = C - O \rightarrow O = C + O$$

Where, M is a metal, e.g. Zn, Ti (n= 2, 4, respectively), or others and *: denotes an excited state.

Phase 2:

The hot gaseous stream leaving the reactor is quenched with water, producing steam that can be used for generating electric power in a turbine[1]. After cooling the effluent to 700 K, the CO-water vapor mixture enters a water-gas shift reactor to produce hydrogen and CO_2 for recycle.

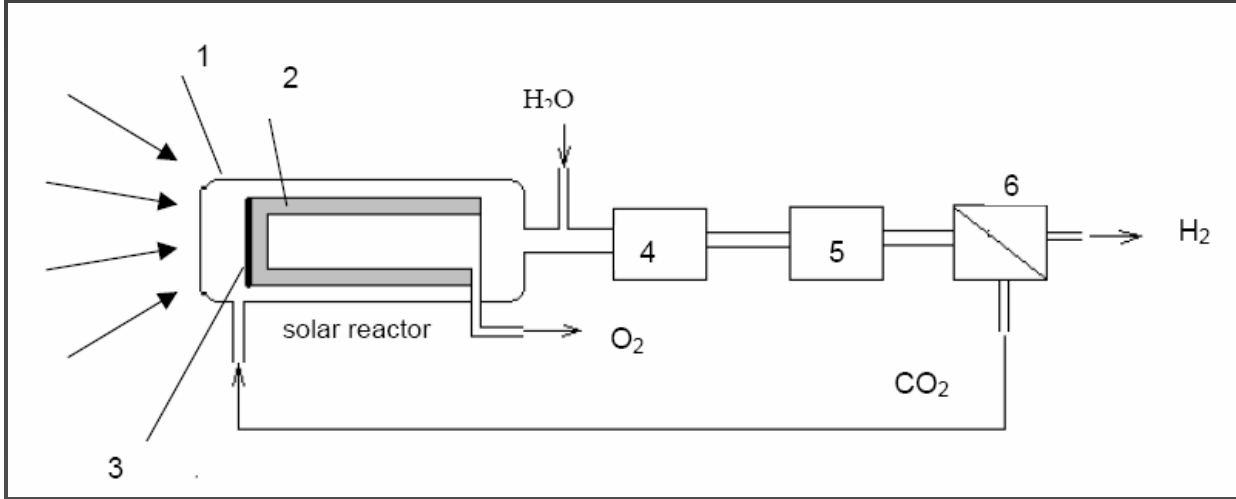

Where:
4- turbine, and
5- water gas shift reactor

Phase 3:

Where:
6-hydrogen-permeable membrane

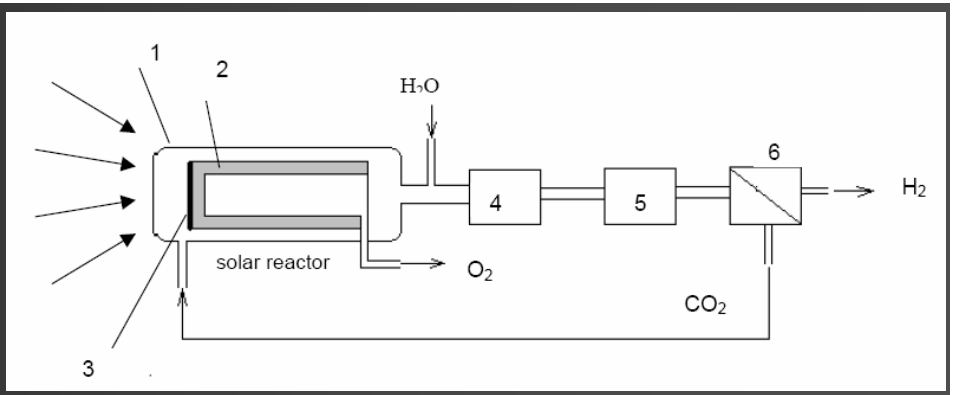

The water-gas shift process (WGS) is a reversible, exothermic reaction which is thermodynamically not favorable at elevated temperatures. To maximize CO conversion and H_2 production, normally the industrial procedures proceeds in two stages using Fe_2O_3 structurally promoted with CrO at 300-500 °C for the high temperature shift and $CuO/ZnO/Al_2O_3$ at 200-250 °C for the low temperature shift. Then, after cooling CO-water vapor mixture down to 500 °C, it passes through the water-gas shift reactor to generate hydrogen and CO_2. The hydrogen-CO_2 mixture is separated by means of a hydrogen-permeable membrane producing high purity hydrogen and CO_2 for recycle.

Membranes

A membrane, inorganic or organic, is a perm-selective barrier between two phases capable of being permeated due to a driving force, that is pressure, concentration or electric field. Inorganic membranes can be divided into porous, microporous and dense and secondly into symmetric and asymmetric. Inorganic membranes are made of alumina, silica, carbon, perovskites, zeria, titania, zeolites and other materials. They are prepared by the ceramic technique, the sol-gel method and other procedures. Porous membranes are those with pores in the mesoporous (2-50 nm) and macroporous (more than 50 nm) domain and microporous membranes are those with pore diameters between about 0.3-2 nm. Dense membranes are those without pores. Porous membranes can be used as supports for the preparation of membranes covered with a microporous material layer and are also used as support for the synthesis of asymmetric membranes with a dense end which could be a metallic thin film or a dense ceramic thin film. The membranes, that will be developed in the frame of the present project are inorganic, asymmetric membranes.

Hydrogen Permeable Membrane

In oxides, during hydrogen absorption, the hydrogen molecule is first dissociated in the surface of the oxide; then, the adsorbed hydrogen atoms are ionized and incorporated directly into the material as protons and electrons, through interaction with the oxide ions and also, by another mechanism, i.e., interstitially located in the tetrahedral and octahedral sites of the perovskite unit cell [2]. The fundamental proton transport mechanism in oxides is the free migration mechanism; where the proton, moves by cation hopping or jumping between immobile host oxygen ions. That is, the proton diffuses by way of molecular orientation and proton displacement or cation (proton) hopping.

2. S. Nieto, R. Polanco and R. Roque-Malherbe, Journal of Physical Chemistry C, 111, (2007) 2809.

Proton Conducting Perovskites

The introduction of defects in some perovskite structures and their distribution in the structure are key factors that determine the protonic conductivity of these materials. In relation with proton transport in perovskites, Iwahara and collaborators were the first to investigate protonic conductivity in $SrCeO_3$ and $BaCeO_3$ doped with trivalent cations such as: Y, Yb, Gd, and Eu [2]. These researchers identified these materials as good high-temperature proton conductors. Thereafter, the corresponding application in solid oxide fuel cells (SOFCs) and other applications were proposed, and extensive research has been carried out in this field.

Proton Conducting Perovskites for Hydrogen Cleaning

Proton conducting powders of $BaCe_{0.95}Yb_{0.05}O_{3-\delta}$, $SrCe_{0.95}Yb_{0.05}O_{3-\delta}$, $BaCe_{0.95}Y_{0.05}O_{3-\delta}$ and $SrCe_{0.95}Y_{0.05}O_{3-\delta}$ perovskites were synthesized using the standard solid-state reaction method [2]. In the case of doped perovskites the perovskite general formula is: $A_{1-y}\,A'_{y}\,B_{1-x}\,B'_{x}\,O_{3-\delta}$

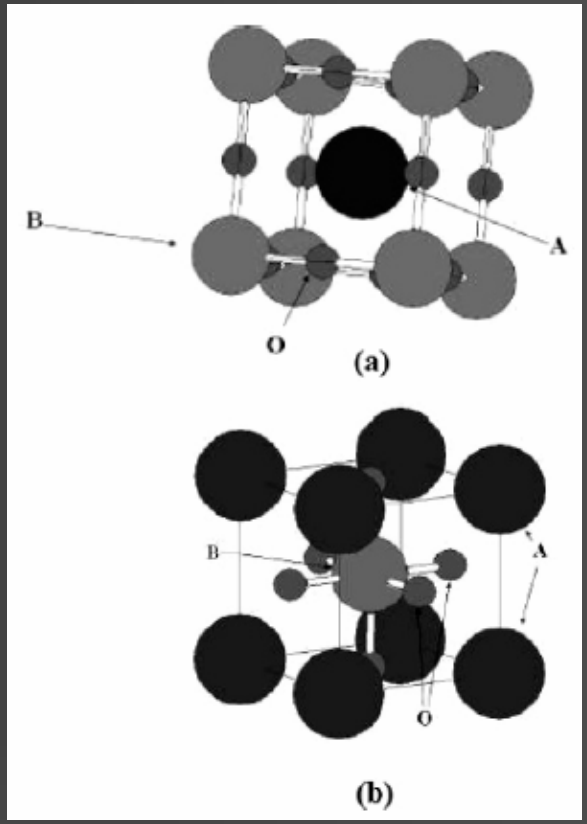

ABO_3 cubic ideal perovskite structure; (a) the center of the cube is occupied by cation A; (b) cation B is placed in the center of the cube [2].

2. S. Nieto, R. Polanco and R. Roque-Malherbe, Journal of Physical Chemistry C, 111, (2007) 2809.

Absorption Kinetics of Hydrogen In Nanocrystals of $BaCe_{0.95}Yb_{0.05}O_{3-\delta}$ Proton-Conducting Perovskite[2]

Powders of $BaCe_{0.95}Yb_{0.05}O_{3-\delta}$ were synthesized using the standard solid-state reaction method. The produced materials were characterized by XRD, SEM, and Raman spectrometry. The absorption kinetics of hydrogen was studied using the TA-TQ500 TGA. The XRD study established the following: the phase composition, cell parameters, and crystallite size. The SEM investigation allowed us to confirm the crystallite size. The Raman study permitted us to confirm the sample phase composition. The absorption study revealed higher absorption magnitudes than those possible if we consider that the proton can only be located in the oxide anions of the perovskite. To explain these results, we proposed that at high temperature the proton could be interstitially located in tetrahedral and octahedral sites because of the increment with temperature of electrons in the conduction band during hydrogen absorption. The enthalpy of absorption, ΔH^0_{ab}, was measured, and it was found that $\Delta H^0_{ab} = 3.6$ eV, a positive value in agreement with the increase with temperature of electrons in the conduction band. Besides, the chemical and self-diffusion coefficients were computed. Subsequently, were calculated the activation energy, E_a, and the pre-exponential factor, D^*_0, using the self-diffusion data. The values obtained were $E_a = 1.6$ eV and $D^*_0 = 0.5 \times 10^{-9}$ m^2/s.

2. S. Nieto, R. Polanco and R. Roque-Malherbe, Journal of Physical Chemistry C, 111, (2007) 2809.

XRD diffraction pattern, Raman Spectrum and SEM micrographies of the $BaCe_{0.95}Yb_{0.05}O_{3-\delta}$ perovskite [2]

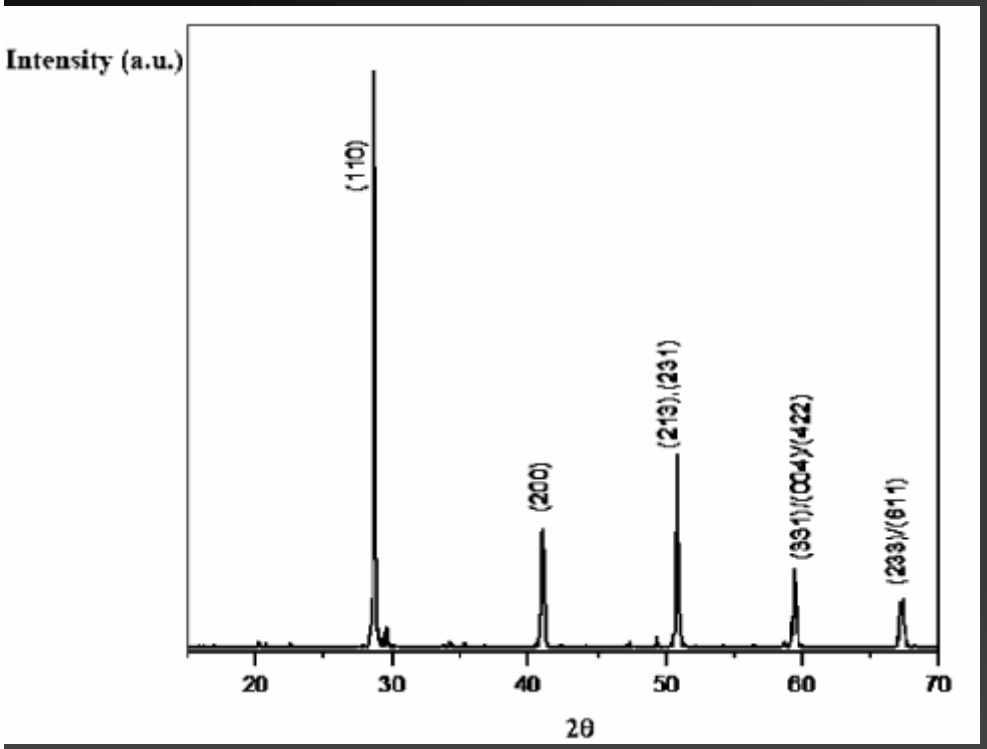

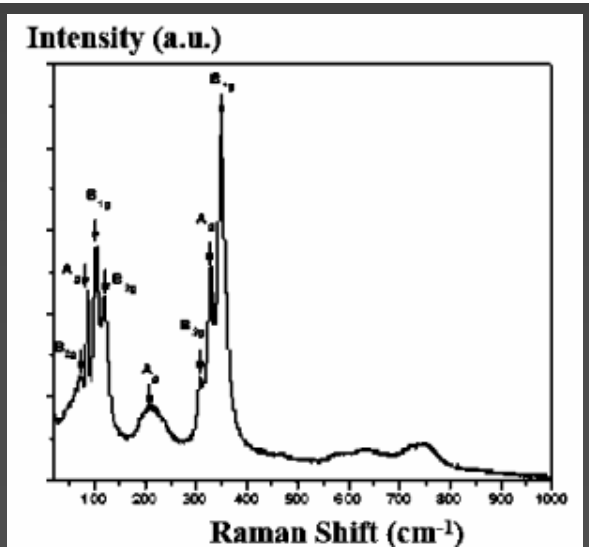

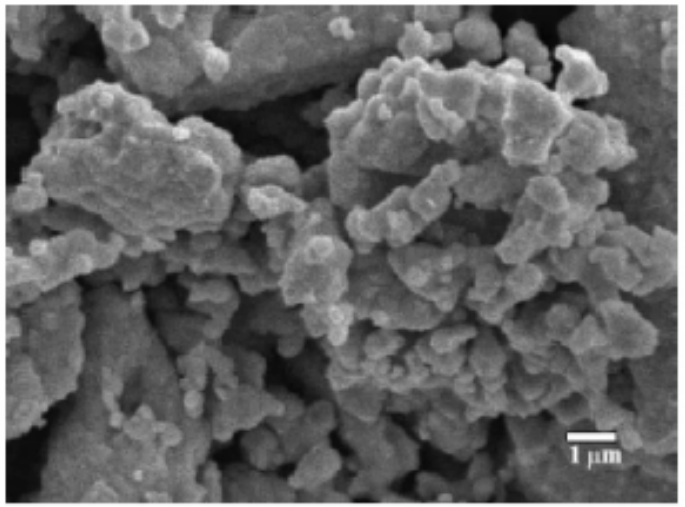

(a)

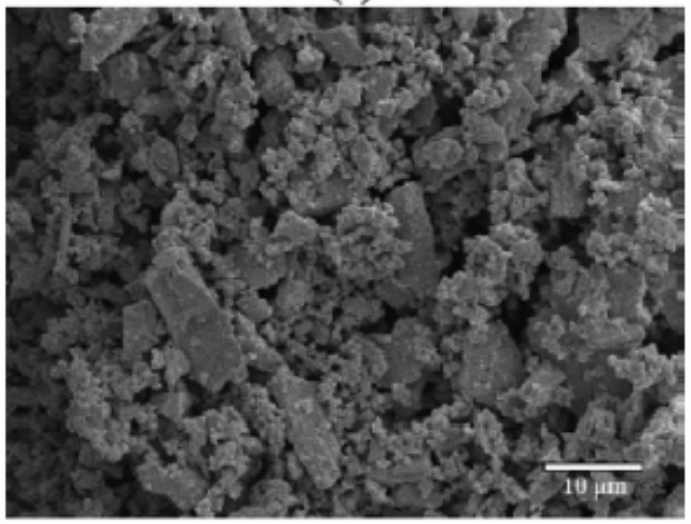

(b)

Absorption Kinetics of H_2 at 1273 K in $SrCe_{0.95}Yb_{0.05}O_{3-\delta}$ [2]

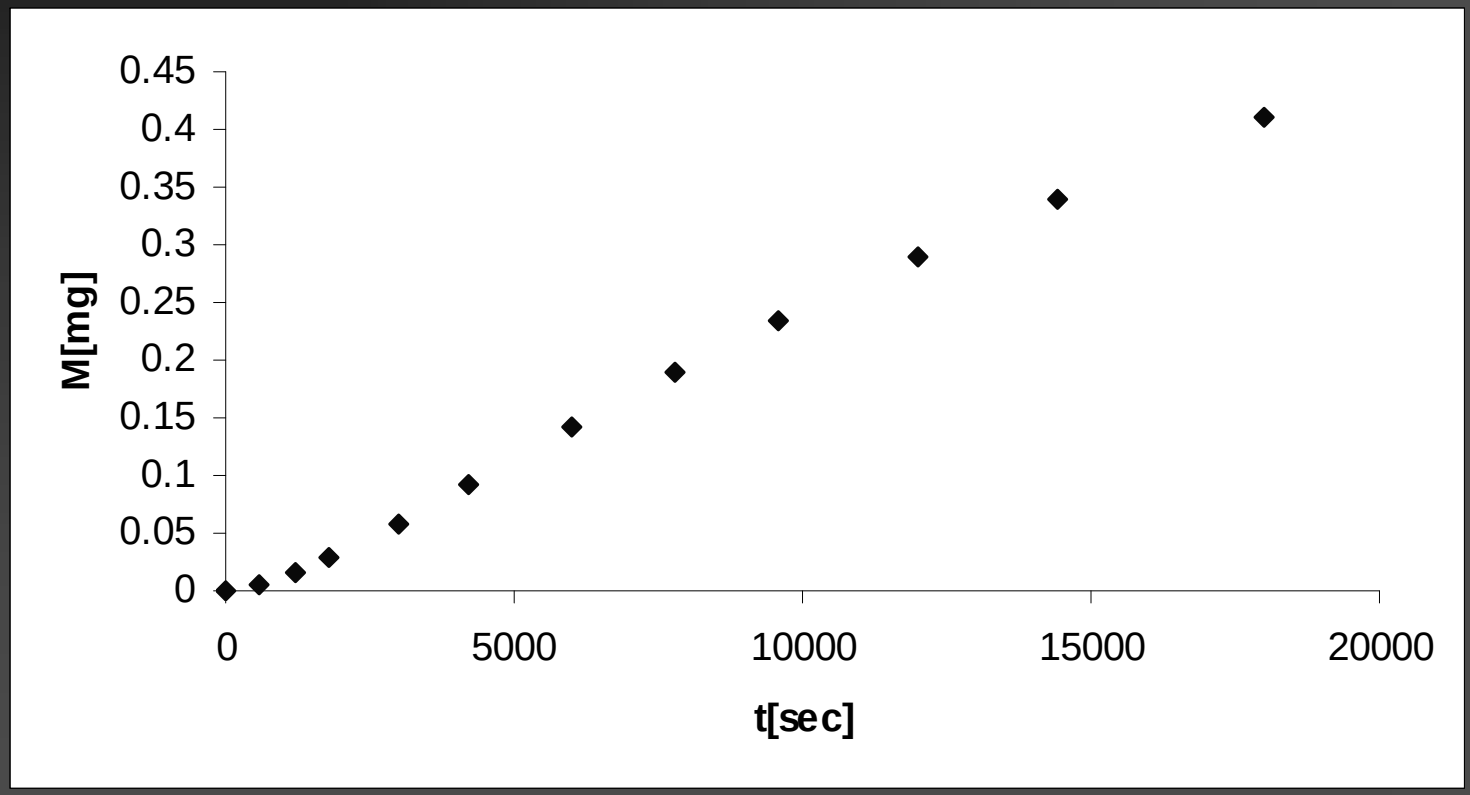

Absorption Kinetics of H_2 at 1173 K in $SrCe_{0.95}Yb_{0.05}O_{3-\delta}$ [2]

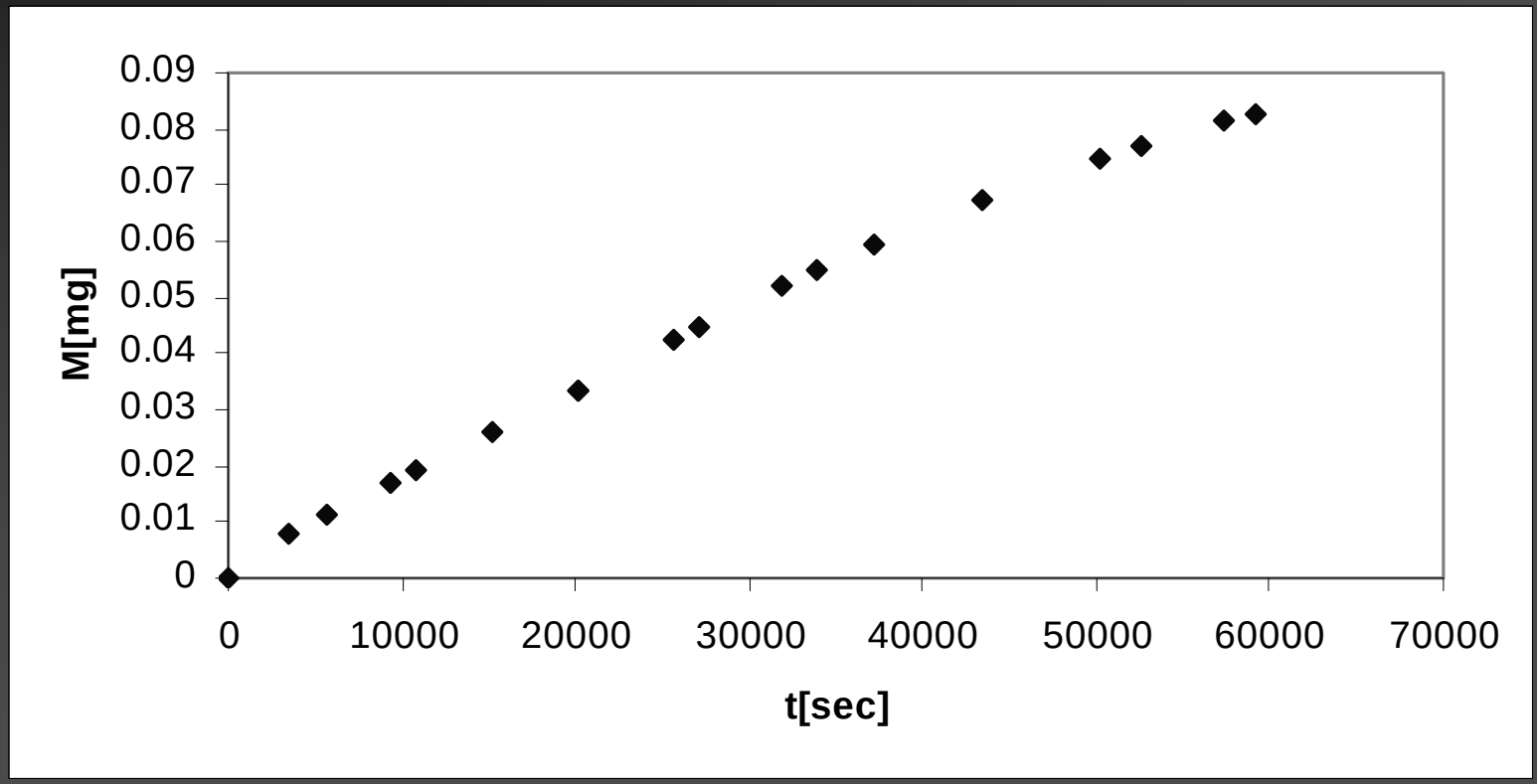

Methodology for the Calculation of the Absorption Kinetics Parameters [2]

The TGA data was collected as a M_t (mg) versus t (s) plot where Mt is the mass of hydrogen absorbed at time t. With the help of the M_t versus t plot, the chemical diffusion coefficient will be evaluated using a solution of Fick's second law for a geometry appropriate for the experimental setup [2]. For the spherical geometry, which is the crystal geometry that we are considering here, and the appropriate, for the experimental setup, boundary and initial conditions, the solution of the Fick's second law is:

$$\frac{M_t}{M_\infty} = 1 - 3\frac{\tilde{D}}{\beta a^2}\exp(-\beta t)\left\{1 - \left(\frac{\beta a^2}{\tilde{D}}\right)^{1/2}\cot\left(\frac{\beta a^2}{\tilde{D}}\right)^{1/2}\right\} + \left(\frac{6\beta a^2}{\tilde{D}\pi^2}\right)\sum_1^\infty\left(\frac{\exp\left(\frac{-\tilde{D}n^2\pi^2 t}{a^2}\right)}{n^2\left[(n^2\pi^2) - \left(\frac{\beta a^2}{\tilde{D}}\right)\right]}\right)$$

where M_t is the mass absorbed at time t, M_∞ is the mass absorbed at equilibrium, and, D, is the chemical diffusion coefficient, a, is the radius of the perovskite crystallite and β is a time constant that describes the evolution of the absortive partial pressure in the dead space of the TGA furnace

Experimental Values of the Mass Absorbed at Equilibrium (M_∞), the Absorption Magnitude (A_m) of H_2 in $BaCe_{0.95}Yb_{0.05}O_{3-\delta}$ at Different Temperatures, and the Sample Weight of the Tested Samples (S_w) [2].

T [K]	1273	1223	1173	1123	1073
M_∞ [mg]	0.52 ± 0.09	0.14 ± 0.03	0.16 ± 0.04	0.005 ± 0.001	0.001 ± 0.001
A_m [wt %]	4.3 ± 0.7	1.3 ± 0.3	1.2 ± 0.3	0.06 ± 0.01	0.01 ± 0.01
S_w [mg]	12.131	10.674	13.304	8.208	10.960

Chemical Diffusion Coefficient and Sample Coverage for Hydrogen Diffusion in the $BaCe_{0.95}Yb_{0.05}O_{3-\delta}$ Perovskite at Different Temperatures [2]

T [K]	$\tilde{D} \times 10^{18}$ [m²/s]	$\theta = A_m/N_A^m$
1273	26 ± 10	1.000
1223	8 ± 3	0.316
1173	7 ± 3	0.289
1123	2 ± 1	0.015
1072	1 ± 1	0.002

2. S. Nieto, R. Polanco and R. Roque-Malherbe, Journal of Physical Chemistry C, 111, (2007) 2809.

Development of Asymmetric Porous-Dense Membranes for Hydrogen Cleanup

The aim of this research project is the synthesis and characterization of inorganic asymmetric membranes, i.e., a dense end plus a porous support, by the combination of the following procedures: sol-gel method, spin coating, and the annealing-sintering method. The dense thin film is prepared by depositing, with the help of the spin coating method, a layer of perovskite crystallites on a ceramic porous membrane made by help the ceramic method of refractory oxides, such as, alumina, silica, silica-alumina or a perovskite, thereafter the compound is heated in order to create the dense end.

Asymmetric Membrane Synthesis Method

The acetates of the different A, B, A' and B' perovskite components are separately dissolved in acetic acid under agitation. Thereafter, all the solutions are mixed together under strong agitation by at least one hour. From the slurry, obtained by the sol-gel procedure, are released several drops over the porous ceramic membrane, located in the spinning bar of the spin coating machine. Thereafter, the assembly powder thin film-porous membrane is heated from room temperature up to 1573 ^{0K} at a rate of 2 ^{0}K/min kept at this temperature by 12 hours and then cooled at the same rate in order to get the perovskite end film over the porous membrane

Laurell Technologies Corporation Spin Coating Machine

Synthesis and Characterization of Zeolite Based Porous Ceramic Membranes [3,4]

Porous membranes were synthesized using a ceramic methodology and characterized by means of XRD, SEM, EDAX and permeation tests. The membranes were produced by thermal transformation of natural clinoptilolite. The XRD study showed clinoptilolite amorphization at 600–900 ^{0}C. A posterior recrystallization to a siliceous phase and a compact aluminosilicate phase at 900–1150 ^{0}C was also produced. The Permeability [B] and Permeance [P] of H_2 and CO_2 were measured using the Darcy Law correlation. It was also applied for gaseous laminar flow using the Carman-Kozeny equation. With the help of this equation the membrane pores sizes were measured. It was shown that the membrane porosity can be controlled by the grain size of the original natural zeolite powder. The membranes were further transformed by hydrothermal synthesis to obtain materials covered with an $AlPO_4$-5 molecular sieve. In conclusion, novel, inexpensive, strong, high permeation rate, and high temperature membranes were produced with natural clinoptilolite, a low cost and available material.

3. R. Roque-Malherbe, W. del Valle, F. Marquez, J. Duconge and M.F.A. Goosen, Separation Science and Technology, 41 (2006) 73.
4. R. Roque-Malherbe, Adsorption and Diffusion of Gases in Nanoporous Materials, CRC Press-Taylor & Francis, Boca Raton, FL, USA, 2007.

Permeation Test Facility [3]

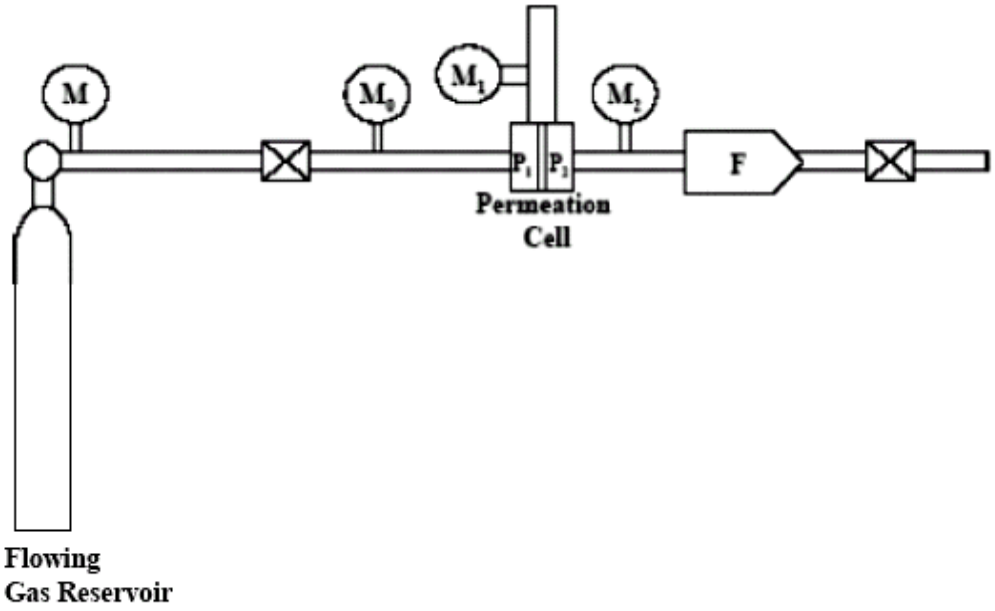

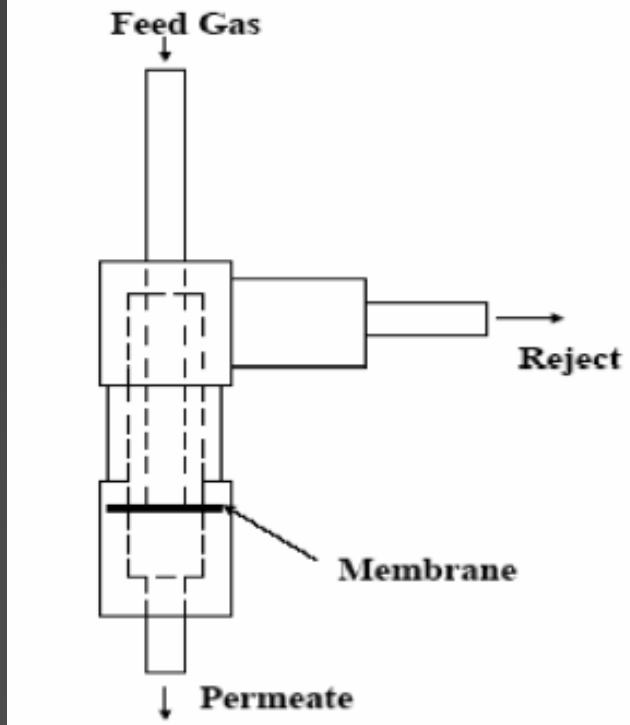

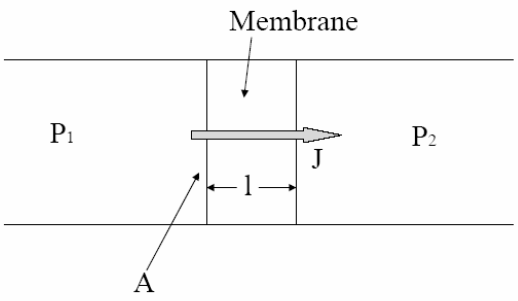

For single gases and a linear pressure drop across the porous media, this transport process follows the Darcy Law:

$$J = B\left(\frac{\Delta P}{l}\right) = \Pi\ \Delta P$$

$$J = \frac{Q}{V_m A}$$

$$\Pi = \frac{B}{l}$$

where: A, is the effective membrane area, B, the Permeability [mol/m s Pa], J, the molar gas flow [mol/m^2 s], l, the membrane thickness, $\Delta P = P_1 - P_2$, the trans membrane pressure [Pa], Π the gas permeance [mol/m^2 s Pa], Q, the gas filtrate flux [m^3/s], and V_m, the molar volume of the flowing gas [m^3/mol], since for an ideal gas: $V_m = \frac{V}{n} = \frac{RT}{P}$.

The permeability for laminar flow, in a real macroporous membrane is described by the Carman-Kozeny equation [3,4]:

$$B_v = \frac{k}{\eta V_m} \quad \textbf{Where:} \quad k \approx \frac{\varepsilon\, d_v^2}{77} \quad \textbf{and} \quad \varepsilon = 1 - \frac{\rho_A}{\rho_R}$$

in which, k, is the permeation factor, in [m^2], η: the dynamic viscosity of the gas in [Pa.s], d_v is the membrane pore diameter, ε, is membrane porosity, ρ_A, the apparent membrane density [g/cm^3], ρ_R, the real membrane density [g/cm^3].

As the membrane pore dimensions decrease, or the mean free path of the molecules increase, the permeating particles tend to collide more with the pore walls than among themselves; then, the Knudsen flow regime is then established, in that case [4]:

$$J_K = \left(\frac{G}{(2MRT)^{1/2}}\right)\left(\frac{\Delta P}{l}\right)$$

$$G = \frac{d_P \varepsilon (\pi)^{1/2}}{2\tau}$$

where, ε, is the porosity, which takes into consideration the fact that transport only takes place throughout the pore and no through the solid matrix. The other effects are grouped together into a parameter called the tortuosity factor, τ,. M, is the molecule mass expressed in molar units and d_p, is the average pore diameter of the porous medium.

Hydrogen and Carbon Dioxide Permeability [B] and Permeance [Π] in the Obtained Membranes [3]

Sample d_p [μm]	Sample treatment temperature [°C]	Sample treatment time [hour]	Gas	$B \times 10^8$ [mol/m.s.Pa]	$\Pi \times 10^6$ [mol/ m^2.s.Pa]
220	700	2	H_2	1.1	4.1
340	700	2	H_2	3.2	11.8
500	700	2	H_2	4.9	18.1
220	800	1	H_2	1.4	5.2
500	800	1	H_2	6.8	25.1
340	800	2	H_2	3.4	12.6
500	800	2	H_2	5.4	20.0
220	700	2	CO_2	0.5	1.8
340	700	2	CO_2	1.0	3.7
500	700	2	CO_2	1.7	6.3
220	800	1	CO_2	0.7	1.7
500	800	1	CO_2	2.4	8.9
340	800	2	CO_2	1.3	5.0
500	800	2	CO_2	2.4	8.9

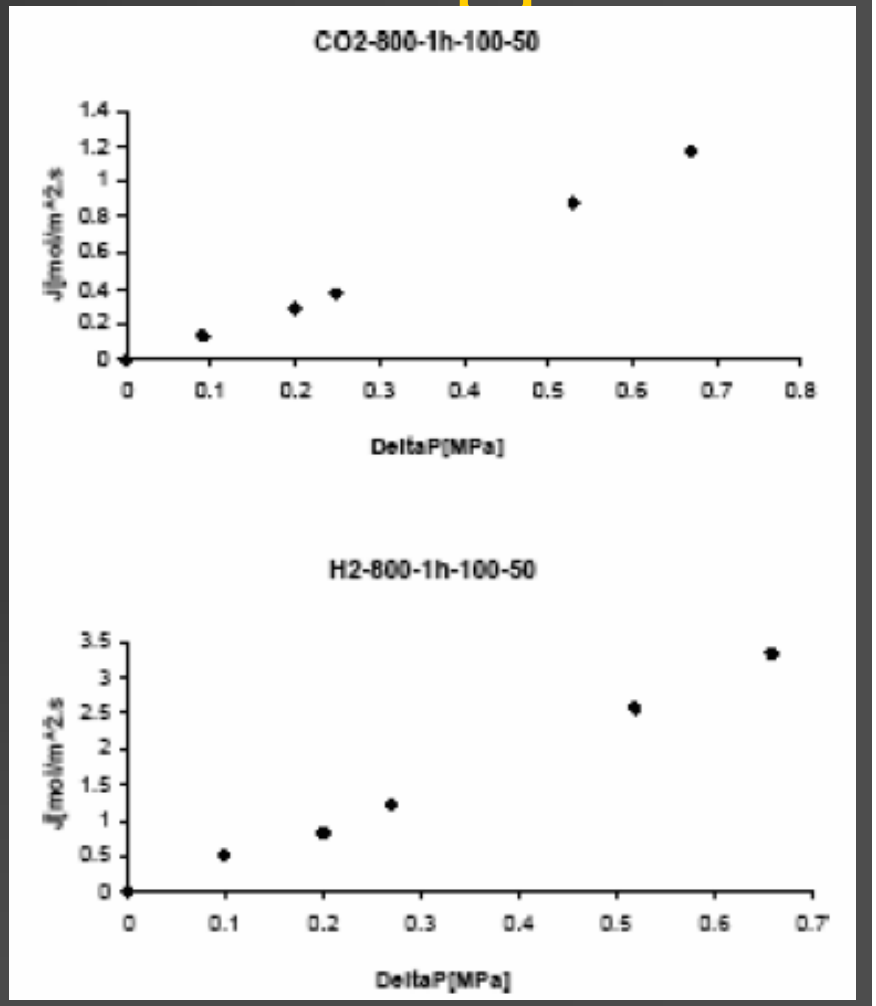

3. R. Roque-Malherbe, W. del Valle, F. Marquez, J. Duconge and M.F.A. Goosen, Separation Science and Technology, 41 (2006) 73.

Hydrogen and Carbon Dioxide Permeation [k] and Membrane Average Pore Diameter [d_v] [3]

Sample d_p [μm]	Sample treatment temperature [°C]	Sample treatment time [hour]	Gas	$k \times 10^{12}$ [m^2]	d_v [μm]
220	700	2	H_2	4.4	32
340	700	2	H_2	12.7	58
500	700	2	H_2	19.4	69
220	800	1	H_2	5.5	38
500	800	1	H_2	27.0	83
340	800	2	H_2	13.5	59
500	800	2	H_2	21.4	74
220	700	2	CO_2	3.4	32
340	700	2	CO_2	6.8	45
500	700	2	CO_2	11.6	58
220	800	1	CO_2	5.1	35
500	800	1	CO_2	16.5	83
340	800	2	CO_2	9.2	62
500	800	2	CO_2	16.5	83

$AlPO_4$-5 Synthesis over a Zeolite Based Membrane [3]

SEM micrographs of ceramic membranes prepared with powders of particle sizes d_p = 100 μm, treated at 900 ^{0}C, (bar 20 μm) (a), and 1100 ^{0}C, (bar 20 μm) (b) and d_p = 500 μm, treated at 800 ^{0}C, during 2 hours (bar 1 μm) (c).

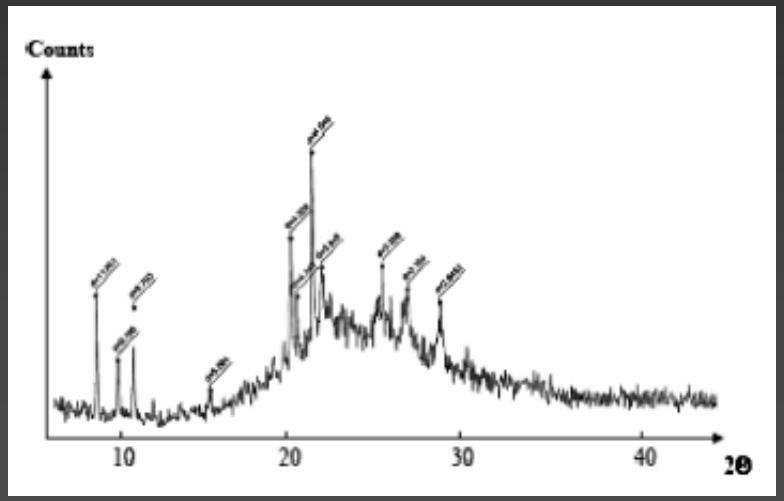

XRD pattern of a ceramic membrane prepared with a clinoptilolite powder of d_p = 500 μ m and treated at 800 ^{0}C during 2 hours and later covered with an AlPO4-5 molecular sieve.

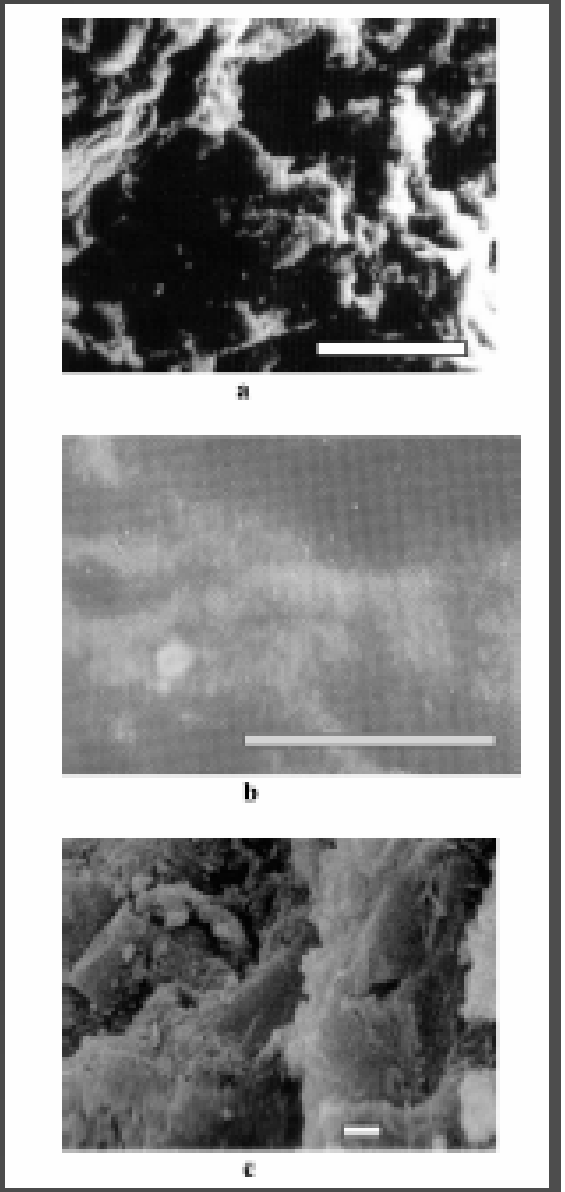

Oxygen Separation

For oxygen cleaning, it is feasible to use oxides having a mixed ionic-electronic conductivity. The ionic component of conductivity (σ_i) in these oxides allows oxygen diffusion through the membrane in the form of O^{2-} ions through the anionic vacancies, via the driving force of a gradient of oxygen chemical potential μ_O , the electronic component σ_e ensures a partial short-circuiting of the concentration cell [1]. The asymmetric membrane materials will be obtained in the form of a dense thin film of the oxygen permeable oxide deposited, by the spin coating method on a refractory ceramic porous membranes made of refractory oxides. The membrane will be tested at the prevailing temperatures (2000-2500 K) and pressures (2-20 atm) in the CO_2 dissociation stage of the cycle.

Perovskites

Ceramic membranes made of perovskite-related phases with the following composition: La-Sr-Co-Fe-$O_{3-\delta}$ have been used successfully in several external conditions owing to their high electronic and ionic conductivity as oxygen permeable membranes, showing fluxes higher than those of the stabilized zirconia (YSZ) at the same temperatures [Peña, M.A. and Fierro, J. L. G. Chem. Review 101 (2001) 1981. The perovskite $SrCo_{0.8}Fe_{0.2}O_{3-\delta}$ (SCF) is reported to provide one of the largest membrane oxygen fluxes in the series $La_{1-y}Sr_yCo_xFe_{1-x}O_{3-\delta}$; consequently, the material of interest to us are those with the highest oxygen permeation fluxes which are obtained for the perovskite with composition $SrCo_{1-x}Fe_xO_{3-\delta}$ with x within the range: $0.2 < x < 0.3$. [G-Y. Adachi, N. Imanaka, and S. Tamura, Chem. Rev., 102 (2002) 2405.

Hydrogen Production by Solid Waste Plasma Thermolysis

IPCAR is part of the project: Hydrogen Production by Solid Waste Plasma Thermolysis. Plasma is the ionized state of matter, it is composed by a gas of charged and neutral particles, formed when ordinary matter is heated over 5,000 ^{0}C. Thermal gasification is the chemical conversion at high temperatures of materials containing carbon atoms into a combustible gas mixture. This gas mixture can be used as a fuel for electric generation.

Plasma Torch

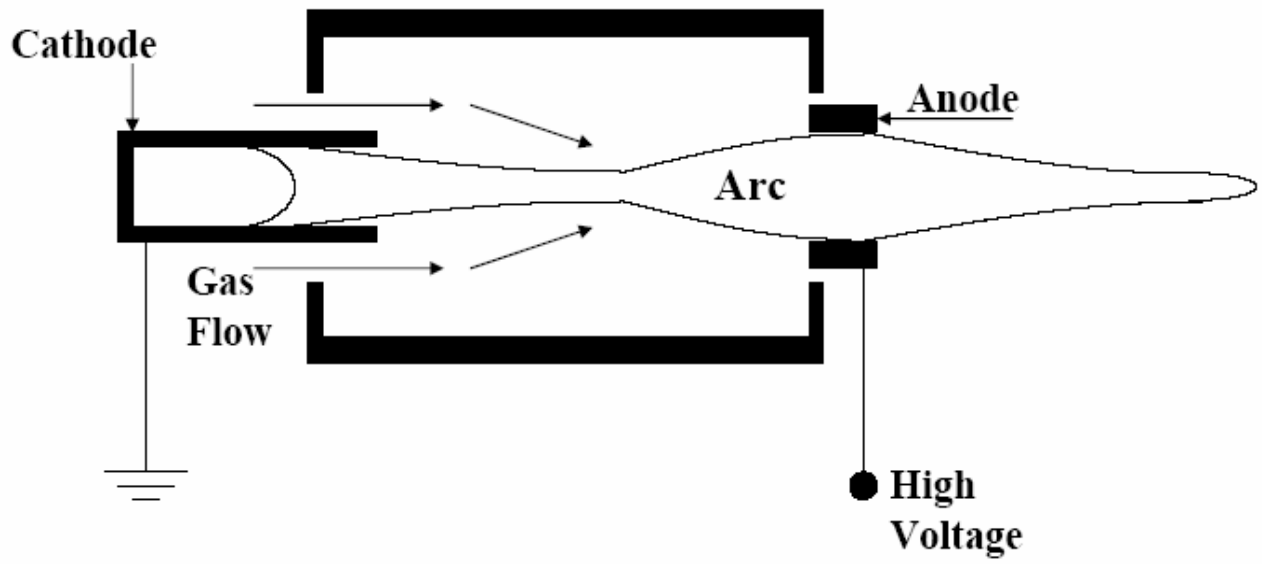

From all the organic components of the solid waste, only simple molecules such as, CO and H_2 (syngas) are produced by the plasma torch. Consequently, a plasma gasification combined cycle plant could produce electrical power using turbines. That is, the previously cleaned syngas can be combusted in simple cycle combustion turbines to generate continuously electricity.

Plasma Torch Gasification and Vitrification of Solid Waste

The plasma torch is a very reliable procedure of producing plasma at atmospheric pressure and temperatures bigger than 5,000 ^{0} C. This methodology allows the dissociation of solid waste, generating, on the one hand: syngas, because the organic materials from all the organic components of the solid waste, becomes molecules of CO and H_2 , i.e. syngas, since only these molecules resist the high temperature of the plasma torch. On the other hand, vitrification is the outcome of the interaction between plasma and the inorganic materials contained in the solid waste. That is, thermal gasification with a plasma torch, dissociates virtually all forms of organic compounds, and melts everything that is not organic. From all the organic components of the used waste, only simple molecules such as, CO and H_2 resist the extremely high temperature of the plasma torch

Puerto Rico Energy Center (PREC) at TU

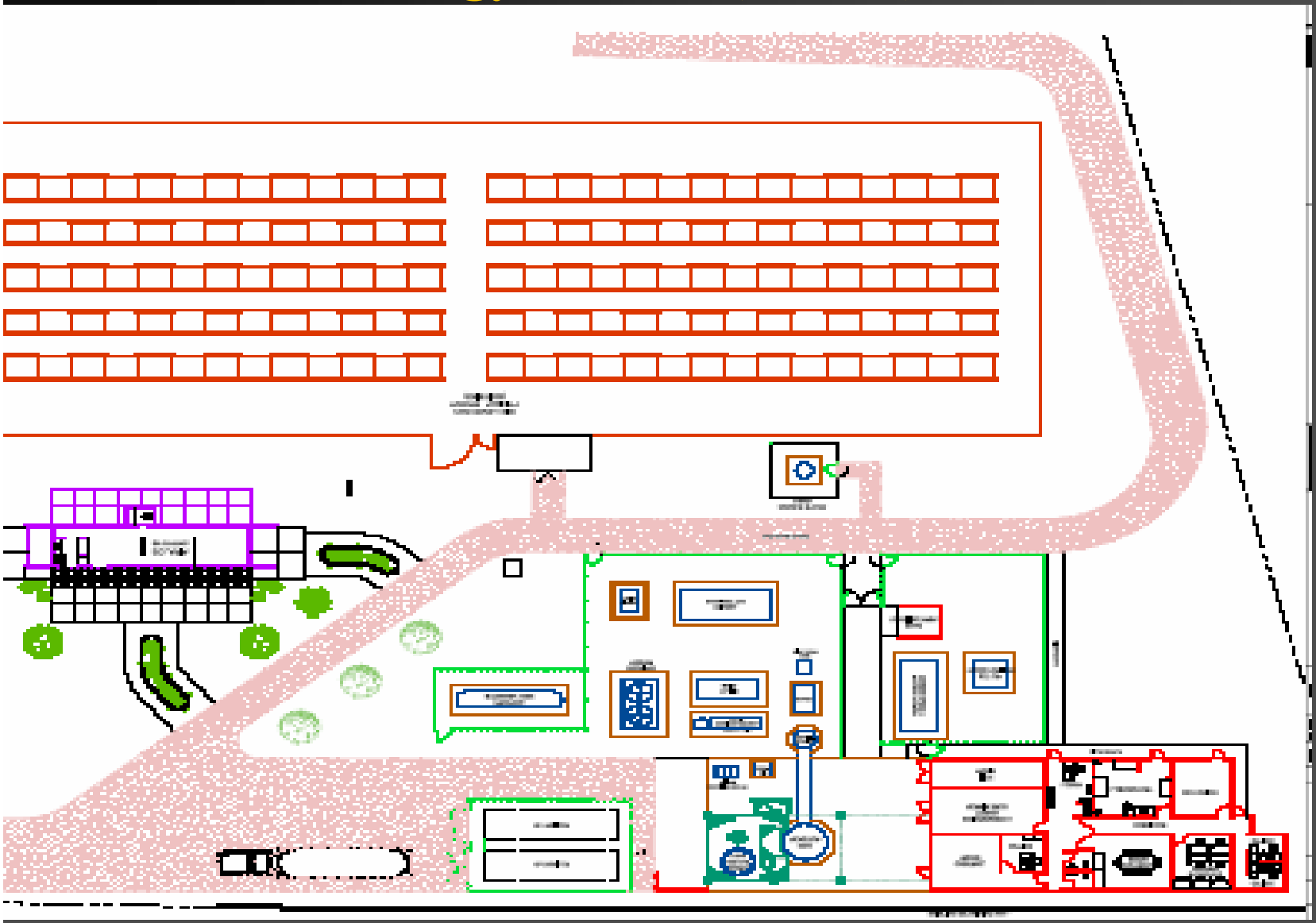

The plasma gasification is developed at the PREC at TU with the participation of the IPCAR

Development of Adsorbents for Hydrogen Storage [4-9]

We have obtained silica nanostrucured materials showing extremely high specific surface area, i.e., up to 2,200 m^2/g (as-synthesized). Our results shows that these materials could adsorb about 11 wt. % of hydrogen contained in the NH_3 molecule. The NH_3 could be later decomposed into H_2 and N_2, with commercial catalysts [4-10].

4. R. Roque-Malherbe, Adsorption and Diffusion of Gases in Nanoporous Materials, CRC Press-Taylor & Francis, Boca Raton, FL, USA, 2007.
5. F. Marquez and R. Roque-Malherbe, Journal of Nanoscience and Nanotechnology (2006) 1114.
6. R. Roque-Malherbe and F. Marquez, Surface and Interface Analysis 37 (2005) 393
7. R. Roque-Malherbe and F. Marquez, Materials Science in Semiconductor Processing 7 (2004) 467
8. R. Roque-Malherbe, F. Marquez, W. del Valle and M. Thommes, Journal of Physical Chemistry-C (Submitted)
9. R. Roque-Malherbe and F. Marquez, Silica Mesoporous Materials, US Patent WO2006052917 – May 18, 2006. IPC: *C01B33/12*; C01B33/00.

SEM micrographs of samples 80 (a) and 68C (b) (bars = 15 000 Å, 10 000 x) and microsphere diameter determined by SEM (D_{SEM}) [6,7].

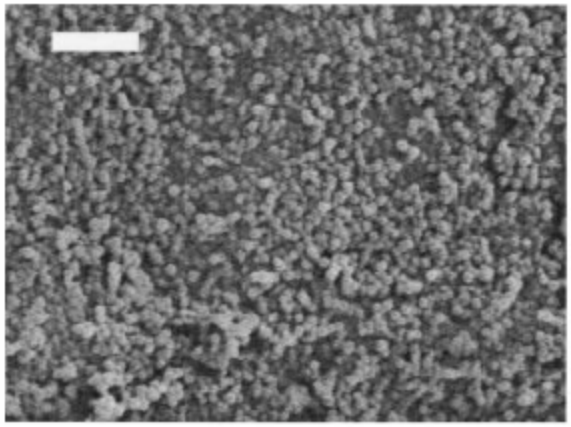

(a)

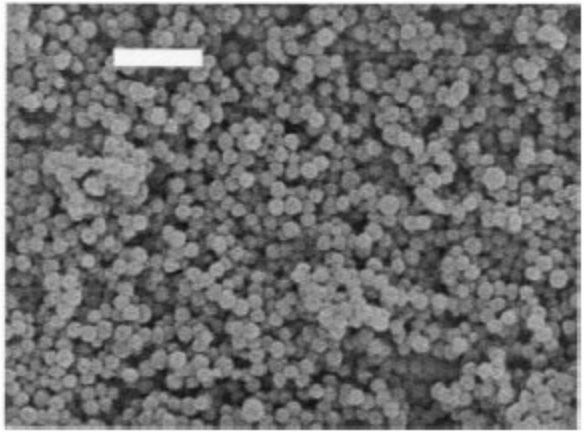

(b)

Sample	D_{SEM} (Å)
68F	500
80	2000
81C	2250
68C	2750
10	3750
68E	4500

Adsorption isotherm of N_2 at 77 K on sample 68F(♦, adsorption branch; ■, desorption branch) and BET-specific surface area (*S*), DFT-pore volume(*W*) and DFT-pore width mode (*d*) corresponding to the synthesized samples and the MCM-41 mesoporous material [6,7]

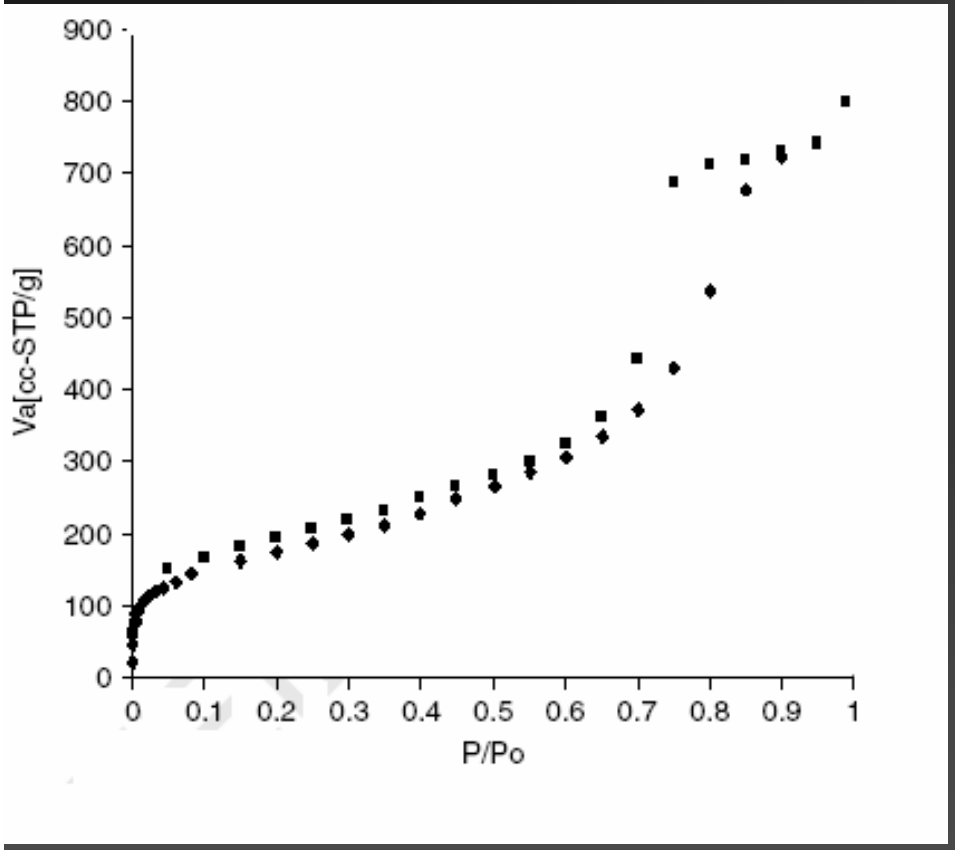

Sample	$S(m^2\ g^{-1})$	$W\ (cm^3\ g^{-1})$	d (Å)
68F	625	1.18	81
80	440	0.49	39
81C	438	0.58	35
68C	320	0.46	21
69B	300	0.52	35
68E	18	0.04	61
MCM-41	820	1.69	35

6. R. Roque-Malherbe and F. Marquez, Surface and Interface Analysis, 37 (2005) 393
7. R. Roque-Malherbe and F. Marquez, Materials Science in Semiconductor Processing 7 (2004) 467.

Adsorption isotherms of N_2 at 77 K in samples (a) 70bs2 and (b) 68bs1E (▲, adsorption branch, and, ■, desorption branch) and Specific Surface Area (S) DFT-Pore Volume (W) and DFT Pore Width Mode (d) of samples synthesized at 300 K (As-synthesized Samples) [5].

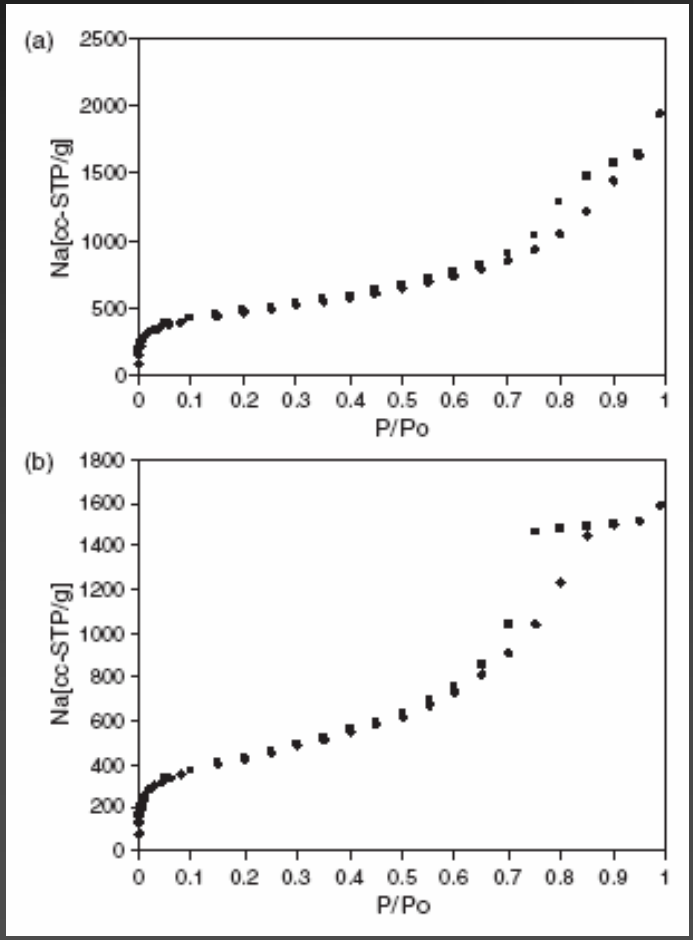

Sample	S [m^2/g]	W_{Mic}[cm^3/g]	W [cm^3/g]	d [Å]
70bs2	1600	0.18	3.0	65
68bs1E	1500	0.27	2.4	81
75bs1	1400	0.16	2.7	125
79bs2	1300	0.21	1.6	31
74bs5	1200	0.14	1.4	61
68C	320	0	0.46	21
MCM-41	800	0	1.7	35

5. F. Marquez and R. Roque-Malherbe, Journal of Nanoscience and Nanotechnology 6 (2006) 1114.

Semi-logarithmic plot of the N_2 adsorption isotherms at 77 K on samples 70bs2-25 (♦) and 70bs2-50 (■) (as-synthesized) [8]

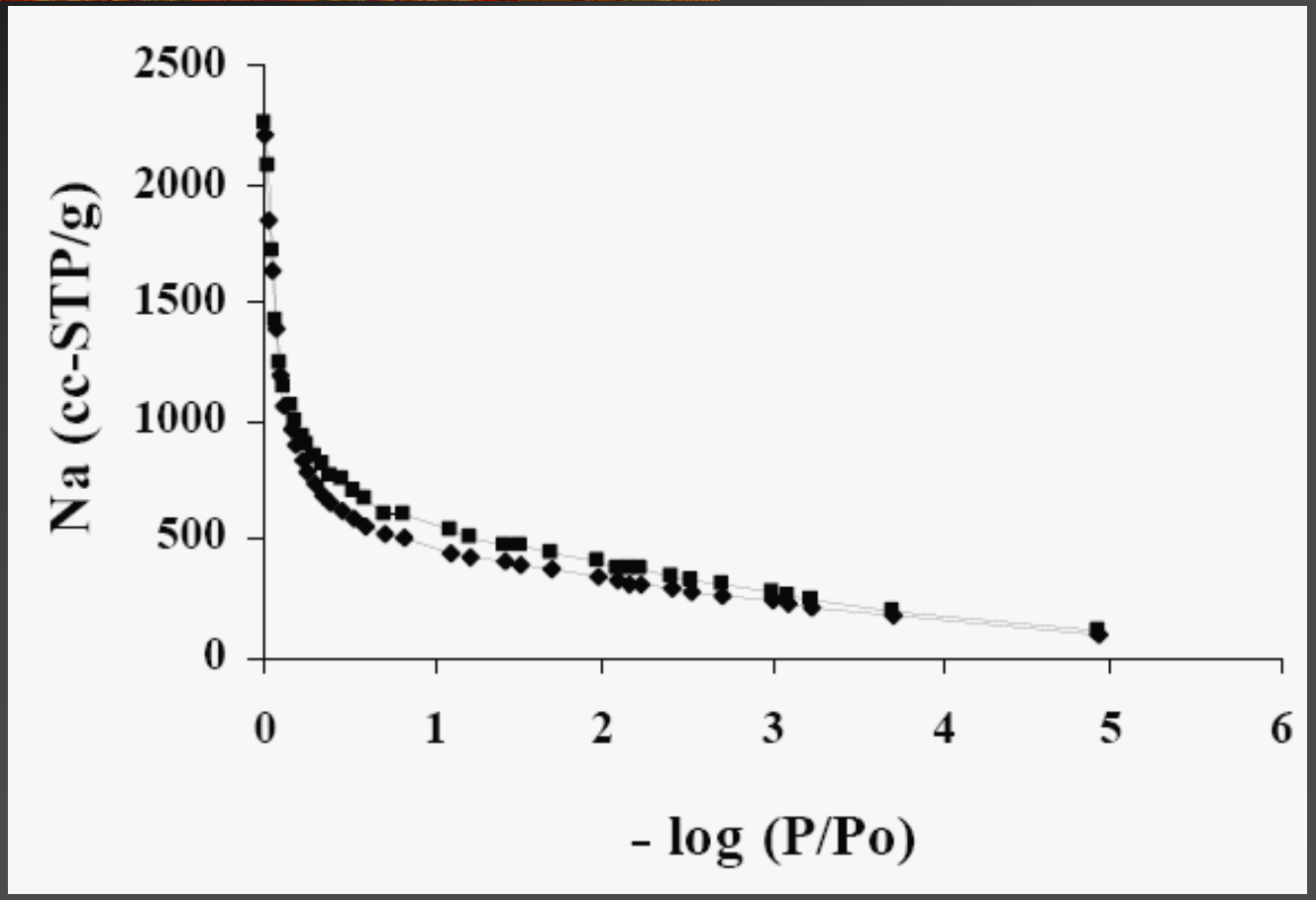

8. R. Roque-Malherbe, F. Marquez, W. del Valle and M. Thommes, Journal of Physical Chemistry-C (Submitted)

Specific Surface Area (S) DFT-Pore Volume (W) and DFT Pore Width Mode (d) of Samples Synthesized at 323 K (As-synthesized Samples) [8]

Sample	S[m^2/g]	W_{Mic}[cm^3/g]	W [cm^3/g]	d [Å]
70bs2-50	2,200	0.25	3.7	66
79bs2-50	1,500	0.25	2.0	36
MCM-41	800	0	1.7	35

BET plots for the adsorption of N_2 adsorption at 77 K on samples: 70bs2-25-s (♦) and 70bs2-50-s (■) [8]

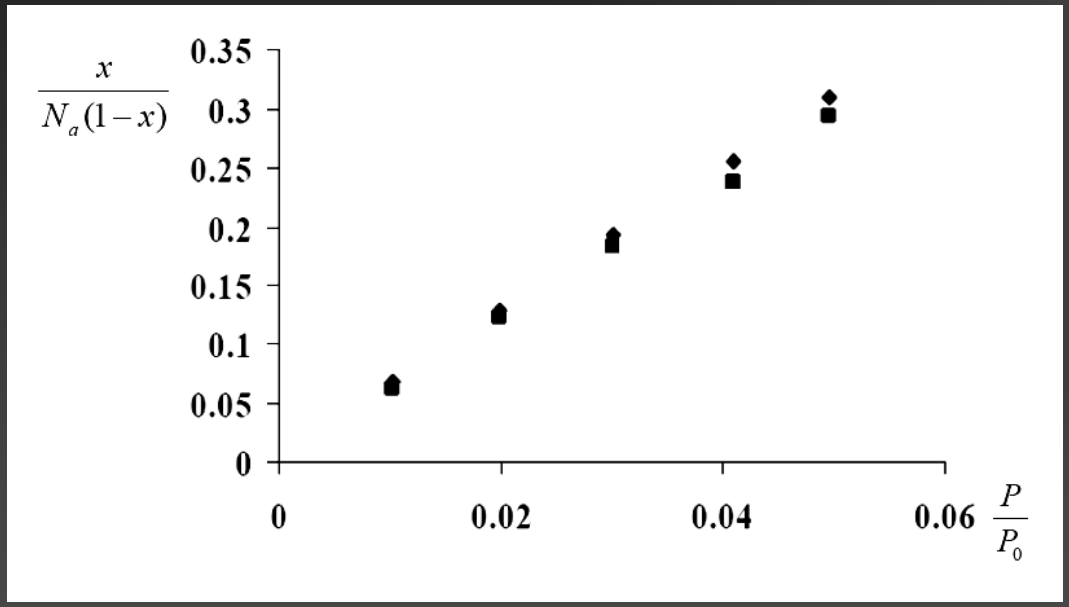

Sample	S [m^2/g]
70bs2-50-s	611
70bs2-25 (a-s)	571

8. R. Roque-Malherbe, F. Marquez, W. del Valle and M. Thommes, Journal of Physical Chemistry-C (Submitted)

Semi-logarithmic plot of the NH_3 adsorption at 300 K on samples 70bs2-25 (♦) and 70bs2-50 (■) [8].

The as-synthesized silica samples after three years of been synthesized, reduced it's specific surfaces up to about 600 m^2/g, that is to say, by about, 1/3 , of the original specific surface area, and become stabilized silica samples. The maximum quantity of hydrogen stored using NH_3 as the hydrogen carrier, at a pressure of about $P = 9.8 \times 10^5$ Pa, that is, that is, $P = 7350$ Torr, namely, a pressure near the vapor pressure of NH_3 at T = 300 K, by the stabilized silica samples was around 11 wt. %, a magnitude higher than the established minimum goal figure of 6.5 wt. %.

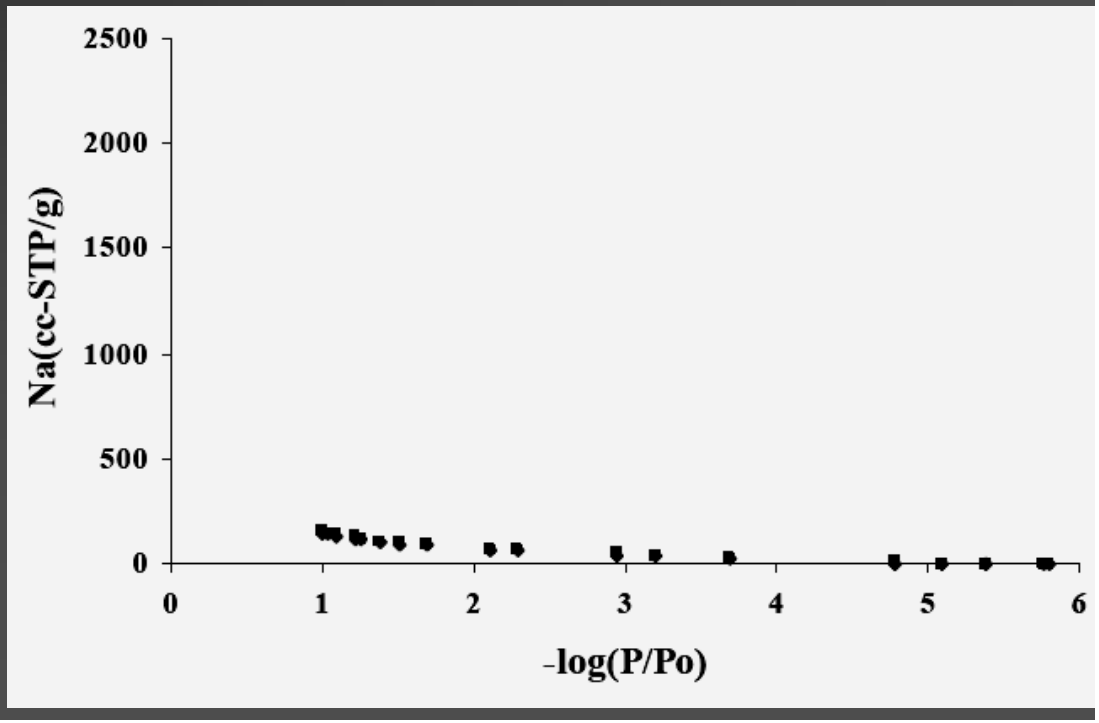

Ionic Exchange in Natural Zeolites [10-14]

The ion exchange reaction in aluminosilicate zeolites is represented by [10,11]:

$$z_B A\{z\} + BZ \leftrightarrow z_A B\{z_B\} + AZ \}$$

Where: $z_A e^+$ and $z_B e^+$ are the charges of cations A and B respectively. $A\{z_A^+\}$ and $B\{z_B^+\}$ describe the cations, *A,* and, *B,* in solution and finally, *AZ* and *BZ* are the cations, *A,* and, *B,* in the zeolite. Ion exchange equilibrium data are reported in the form of isotherms with the help of the equivalent ionic fraction [23]; in solution (see the figure):

$$X_A = \frac{z_A m_A}{z_A m_A + z_B m_B} \quad \text{and} \quad X_B = \frac{z_B m_B}{z_A m_A + z_B m_B}$$

10. R. Roque-Malherbe, W. del Valle and E. Menendez, Removal of heavy metals from Water Solutions by Dynamic Ionic Exchange, in Na-Clinoptilolite Beds. US Provisional Patent Application, Registration No.: 34,542, May 17, 2002. Presented in final form in October 2006

11. R. Roque-Malherbe, Applications of Natural Zeolites In Pollution Abatement and Industry. In, Handbook of Surfaces and Interfaces of Materials, Volume 5, Editor H. S. Nalwa, Academic Press, New York, Chapter 12, pp. 495-522, 2001.

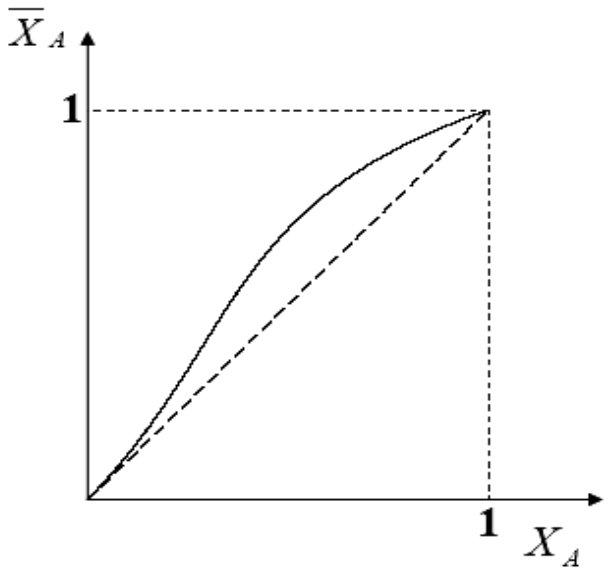

HEU Type Framework [4, 11]

The structure of clinoptilolite (HEU framework type) show 3 channels. One 8-MR channel along [100], with an access of 2.6 A x 4.7 A. Two parallel channels along [001] one 8-MR with a window of access with 3.3 A x 4.6 A, and a 10-MR with an access of 3.0 A x 7.6 A (see the figure) [4, 11].

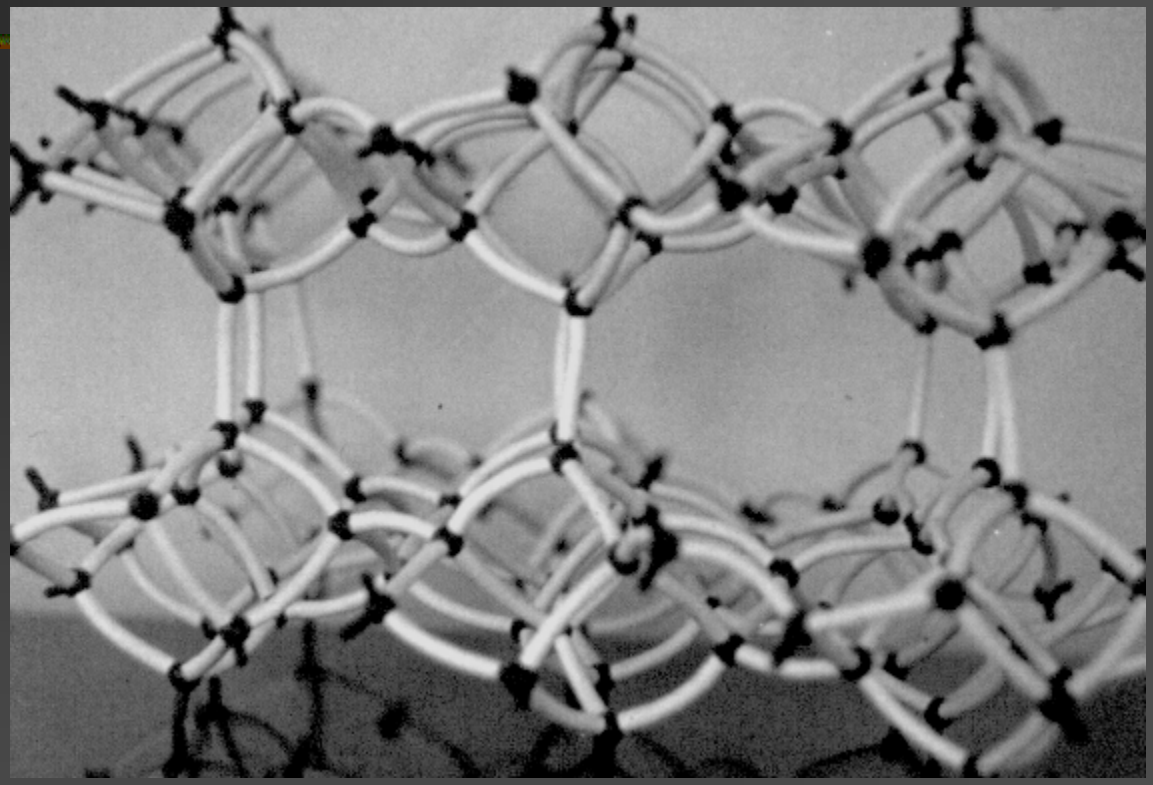

4. R. Roque-Malherbe, Adsorption and Diffusion of Gases in Nanoporous Materials, CRC Press-Taylor & Francis, Boca Raton, FL, USA, 2007.
11. R. Roque-Malherbe, Applications of Natural Zeolites In Pollution Abatement and Industry. In, Handbook of Surfaces and Interfaces of Materials, Volume 5, Editor H. S. Nalwa, Academic Press, New York, Chapter 12, pp. 495-522, 2001.

The Plug Flow Ion Exchange Reactor (PFIER) [10,11]

The plug flow model signifies that the fluid velocity profile is plug shaped, explicitly, is uniform at all radial positions, as was explained for the plug flow adsorption reactor [4,10]. The fixed-bed ion exchange reactor, as well, is packed randomly with particles of a solid ion exchanger which are clean, or just regenerated. The ion exchange process is supposed to be very fast relative to the convection, and diffusion effects, subsequently local equilibrium will exist close to the ion exchange beads. Further assumptions are that no chemical reactions occur in the column, and that only mass transfer by convection is significant. The operation of an ion exchanger in dynamic conditions is characterized by the total exchange capacity, the selectivity and the kinetics of the ion exchange process and also by the mechanical properties of the exchanger material. The zeolite bed in the Plug Flow Ion Exchange Bed Reactors (PFIER) could be divided in three zones: I the equilibrium zone, II Mass Transfer Zone (MTZ) with a length, D_o and III the unused zone [4,10]. The PFIER has a cross sectional area, S, column length, D, and ion exchanger mass in the bed, M, (see figure). This PFIER operate in steady state regime and through it is passing a volumetric flow rate [4]:

$$F = \frac{\Delta V}{\Delta t} = \frac{volume}{time}$$

Of an aqueous solution with an initial concentration $C_A^0 \left(\frac{mass}{volume}\right)$ of cation, A, with charge z_A^+.

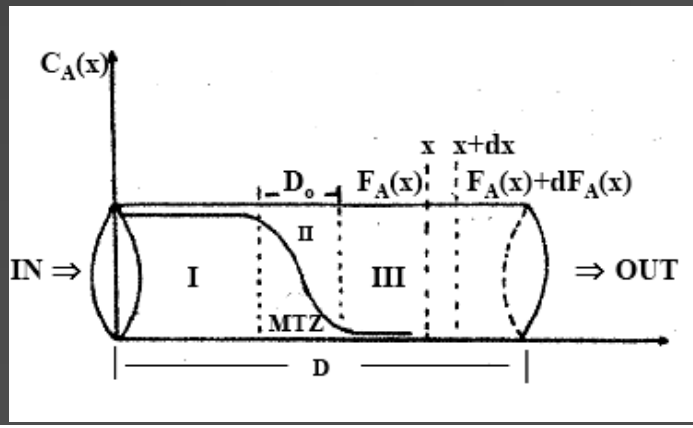

Breaktrough Curve

The output of the operation of the PFIER is a breakthrough curve (see the figure) [4,10]; where: C_A^0, is the initial concentration, C_A^e, is the breakthrough concentration, V_e, is the fed volume, of the aqueous solution of the electrolyte solution to breakthrough, and, V_b, is the fed volume to saturation. This is a response curve where it is exposed the relation between concentration at the exit of the packed bed ion exchange reactor during time.

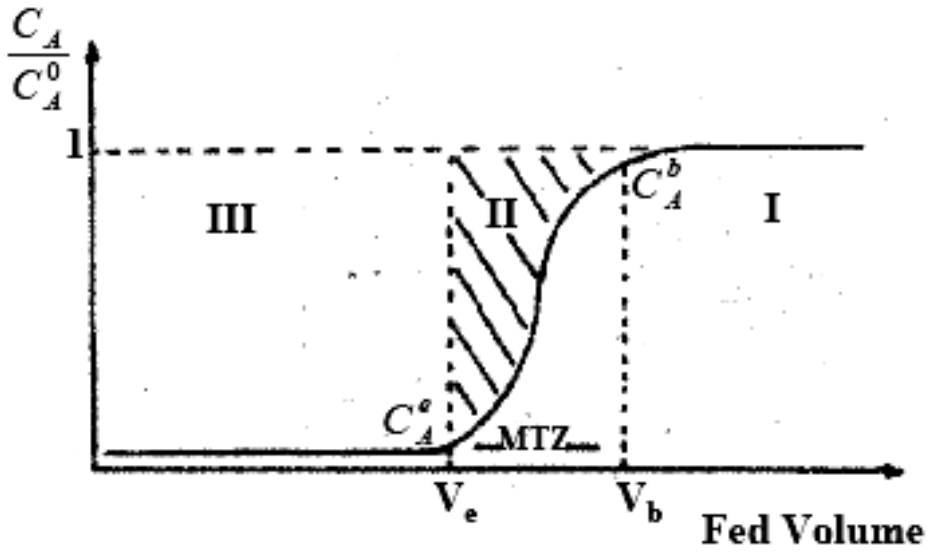

Parameters Characterizing the Operation of the PFIER

The length of the Mass Transference Zone (MTZ), D_o, is defined by the following expression [10]:

$$D_0 = 2D\left[\frac{V_b - V_e}{V_b + V_e}\right]$$

The volume of the empty bed is, $V_B = \varepsilon V$, where, V, is the bed volume, and, ε, is the fraction of free volume in the bed, and the interstitial fluid velocity, u is defined as [4,10]:

$$u = \frac{F}{S}$$

In addition, the contact or residence time of the fluid passing though the reactor, τ, is calculated with equation [4,10]:

$$\tau = \frac{V_B}{F}$$

Other parameters characterizing a PFIER are the column breakthrough capacity, B_C, the column saturation capacity, S_C, an the column efficiency, E, of the PFIEBR which are calculated with the following equations [10]:

$$B_C = \frac{C_A^0 V_e}{M}$$

$$S_C = \frac{C_A^0 V_b}{M}$$

$$E = \frac{B_C}{S_C}$$

Cationic Exchange in a Plug Flow Reactor Packed with Clinoptilolite

In the figure is shown the experimental breakthrough curve obtained during the operation of the tested PFIEBR filled with a mass of: $M = 1.5\ g$ of homoinic Na-clinoptilolite with a grain size, ϕ, of 0.6 mm to 0.8 mm with a flow rate: $F = 0.8\ \frac{cm^3}{min}$, of aqueous solutions of $Pb(NO_3)_2$ with an initial concentration: $C^0_{Pb^{2+}} = 0.45\ \frac{mg}{cm^3}$ of Pb^{2+} [10,12,13].

12. R. Roque-Malherbe, W. del Valle, J. Ducongé, and E. Toledo, International Journal of Environment and Pollution Vol. 28 (2006).
13. R. Roque-Malherbe, W. del Valle, N. Planas, K. Gómez, D. Ledes, L. Garay and J. Ducongé, Zeolites '02 Book of Abstracts (P. Misaelides Ed.) 7th International Conference on the Occurrence, Properties and Use of Natural Zeolites, Thessaloniki, Greece, June 3-7, 2002. pp. 316-317.
14. R. Roque-Malherbe, Physical Chemistry of Materials (Book in Progress)

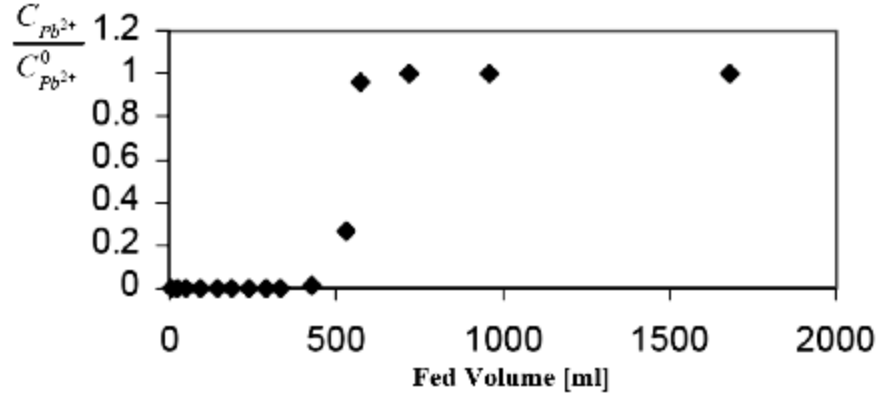

Operational parameters of the tested PFIER [10,12,13]

Cation	τ [sec]	B_C $\left[\frac{mequiv}{g}\right]$	D_o [cm]	E [%]	F $\left[\frac{cm^3}{min}\right]$	ϕ [mm]
Pb^{2+}	75	0.42	3.5	32	0.80	0.8-2
Pb^{2+}	60	1.25	1.0	75	0.80	0.6-0.8
Ni^{2+}	< 60	0.00	> 3.7	0	0.80	0.8-2
Ni^{2+}	148	0.30	3.3	40	0.32	0.6-0.8
Ni^{2+}	60	0.27	3.4	35	0.80	0.6-0.8
Co^{2+}	148	0.27	2.3	51	0.32	0.6-0.8
Cu^{2+}	148	0.57	2.1	52	0.32	0.6-0.8
Cu^{2+}	75	0.45	2.4	50	0.80	0.6-0.8

Note: The errors in τ, B_C, D_o, E and F are $\pm$ 10 sec, 0.05 mequiv/g, $\pm$ 0.3 cm, $\pm$ 5 % and 0.02 cm^3/min respectively.

The Modular Canister PFIER

With the help of the equation [10]:

$$2D\left[\frac{V_b - V_e}{V_b + V_e}\right] = \frac{u}{k}\ln\left(\frac{C_A^0}{C_A^e}\right)$$

Which was obtained using the PFIER model, where the parameters: D, V_B, V_e, u, C_A^0 and C_A^e, were previously defined and, k, is the coefficient in the rate equation:

$$r_A = k[C(x)]$$

Where: $r_A\left[\frac{mass}{Volume - Time}\right]$, is the rate of the reaction producing the accumulation of the cations of atom A in the zeolite, was calculated the maximum, D_o with the help of the following equation [10]:

$$D_0 = \frac{u}{k}\ln\left(\frac{C_A^0}{C_A^e}\right)$$

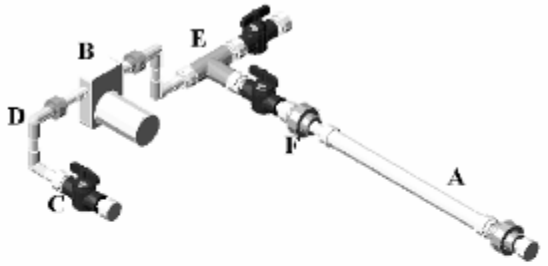

a

b

Synthesis and Characterization of Low Refractive Index Aerogel Silica for Cherenkov Counters

The aim of this research project is to investigate the properties and potential applications of extremely high surface area silica materials as low refractive index and high transparency aerogel silica for Cherenkov counters.

Active Research Grants and Special Projects

- Synthesis and Characterization of Low Refractive Index Aerogel Silica for Cherenkov Counters, DOE-Massie Chair Project (DoE, $ 420,000 four years).
- Water Splitting with Quantum Boost (DoE, funding initially approved as sub grantee $ 400,000, but not yet received)
- Strengthening of Modern Physics Laboratory,

  ($ 84,000, 2005-06 DoD-HIS)
- Turabo University Publications and Presentations Award, $ 24,000 (2004-2007)

Grants Pending Review

- **Ammonia Adsorption on Nanostructured Silica Materials for Hydrogen Storage, NSF**

Past Research Grants and Special Projects (2002-2006):

- 5. Hydrogen Diffusion in $BaCe_{2.95}Yb_{0.05}O_3$ (DoE, Massey Chair project, $210,000, during one year (2005-2006).
- 4. Synthesis and Porosity Characterization of Membranes for Gas Cleaning, (NASA Research Grant, $ 215,000) (2003-2004)
- 3. Amgen Manufacturing Limited Site Service Agreement, Participant, $750,000 (2002-2003).
- 2. Liquid Chromatography-Mass Spectrometry Laboratory, Waters Technologies Corporation, Puerto Rico Branch, $ 339,000 (2000-2003).
- 1. Development and design methodology for the construction of ionic exchange modular canisters, MIE-NSF, $15,000 (2002).

Research Projects in Progress

- Ethanol Production by Zeolite “Catalyzed” Fermentation
- Hydrogen Production from Ethanol
- Synthesis of All-silica Zeolites for the Removal of Organic Compounds from Waste Waters